Intermolecular Interactions in Dye-Sensitized Solar Cells: A Computational Modeling Perspective

ARTICLE *in* JOURNAL OF PHYSICAL CHEMISTRY LETTERS · MARCH 2013

Impact Factor: 7.46 · DOI: 10.1021/jz302147v

2 AUTHORS:

Mariachiara Pastore
Italian National Research Council
52 PUBLICATIONS **1,248** CITATIONS
SEE PROFILE

Filippo De Angelis
Università degli Studi di Perugia
265 PUBLICATIONS **11,207** CITATIONS
SEE PROFILE

THE JOURNAL OF PHYSICAL CHEMISTRY Letters

Perspective

pubs.acs.org/JPCL

Intermolecular Interactions in Dye-Sensitized Solar Cells: A Computational Modeling Perspective

Mariachiara Pastore* and Filippo De Angelis*

Computational Laboratory for Hybrid Organic Photovoltaics (CLHYO), Istituto CNR di Scienze e Tecnologie Molecolari, via Elce di Sotto 8, I-06123 Perugia, Italy

Supporting Information

ABSTRACT: We present a unified overview of our recent activity on the modeling of relevant intermolecular interactions occurring in dye-sensitized solar cells (DSCs). The DSC is an inherent complex system, whose efficiency is essentially determined by the interrelated phenomena occurring at the multiple molecular−semiconductor−electrolyte heterointerfaces. In this Perspective, we illustrate the basic methodology and selected applications of computational modeling of dye−dye and dye−coadsorbent intermolecular interactions taking place at the dye-sensitized interface. We show that the proposed methodology offers a realistic picture of aggregation phenomena among surface-adsorbed dyes and nicely describes semiconductor surfaces cosensitized by different dyes. The information acquired from this type of studies might constitute the basis for an integrated multiscale computational description of the device functioning, including all of the possible interdependencies among the device constituents, which may further boost the DSCs efficiency. We believe that this direction should be the target of future computational research in the DSC field.

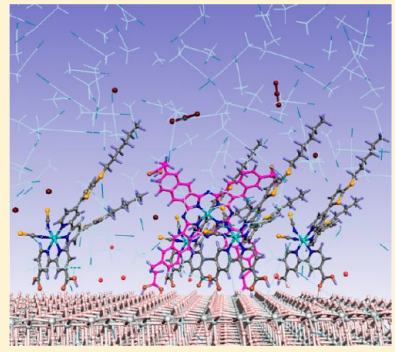

Dye-sensitized solar cells (DSCs) are photoelectrochemical cells that directly convert sunlight into electrical energy at low cost and with high efficiency.[1−4] This has stimulated intensive academic and industrial research, with the recent launch of the first DSCs-based commercial product highlighting the market potential of this technology. Crucial to the DSCs' functioning is the photoinduced charge separation occurring at the heterointerface(s) between a dye-sensitized nanocrystalline, mesoporous metal oxide electrode, and a redox shuttle in an electrolyte solution or hole conductor, generally referred to hereafter as the redox shuttle.

Dye−dye intermolecular interactions are of paramount importance in determining the overall DSCs conversion efficiency.

The heart of the device consists of a mesoporous oxide layer, which is deposited onto a transparent conducting oxide on a glass or plastic substrate; see Scheme 1. Grafted on the surface of the nanocrystalline oxide is a monolayer of sensitizing dye, which absorbs the solar radiation and injects the ensuing photoexcited electrons into the manifold of unoccupied semiconductor states, which we refer to as the conduction band (CB); the concomitant hole created on the dye is transferred to the redox shuttle, which is in turn regenerated by a catalyst at the counter electrode, closing the circuit (Scheme 1). The DSCs efficiency is defined as

$$\eta = \frac{V_{oc} J_{SC} \mathrm{FF}}{P_I} \quad (1)$$

where V_{oc} (the open-circuit voltage of the cell) is the difference between the quasi-Fermi level of the semiconductor under illumination and the redox potential of the mediator (Scheme 1), J_{SC} is the photocurrent density at short circuit, FF is the fill factor, and P_I is the intensity of the incident light. The overall DSCs' performance is strongly determined by the efficiency of the various desired electron-transfer and charge-transport processes against the recombination losses occurring between electrons in the semiconductor and oxidized dyes and/or oxidized species in the redox shuttle.

DSCs can be schematized as being formed by three fundamental components (i.e., the dye, the metal oxide, and the redox shuttle), which, to a first approximation, can be individually optimized in the continuing search for higher photovoltaic efficiency or longer device temporal stability.

Ru(II)−polypyridyl complexes have been primarily employed as dye sensitizers.[5−9] The remarkable performance of the N3 dye,[5] of its doubly protonated analogue (N719),[6] and of the so-called black dye or N749[7,8] had a central role in significantly advancing the DSCs' technology, with solar to electric power efficiencies exceeding 11%.[6,9] In the last years, a flourishing family of new-generation Ru(II) dyes have been designed and synthesized to provide a higher molar extinction

Received: December 22, 2012
Accepted: February 28, 2013
Published: February 28, 2013

Scheme 1. (Left) Schematic Representation of the Constituent Materials and Energy Levels of a DSC[a]; (Right) Diagram of a 1 nm Slab Sliced from a Pore in a Typical DSC[b]

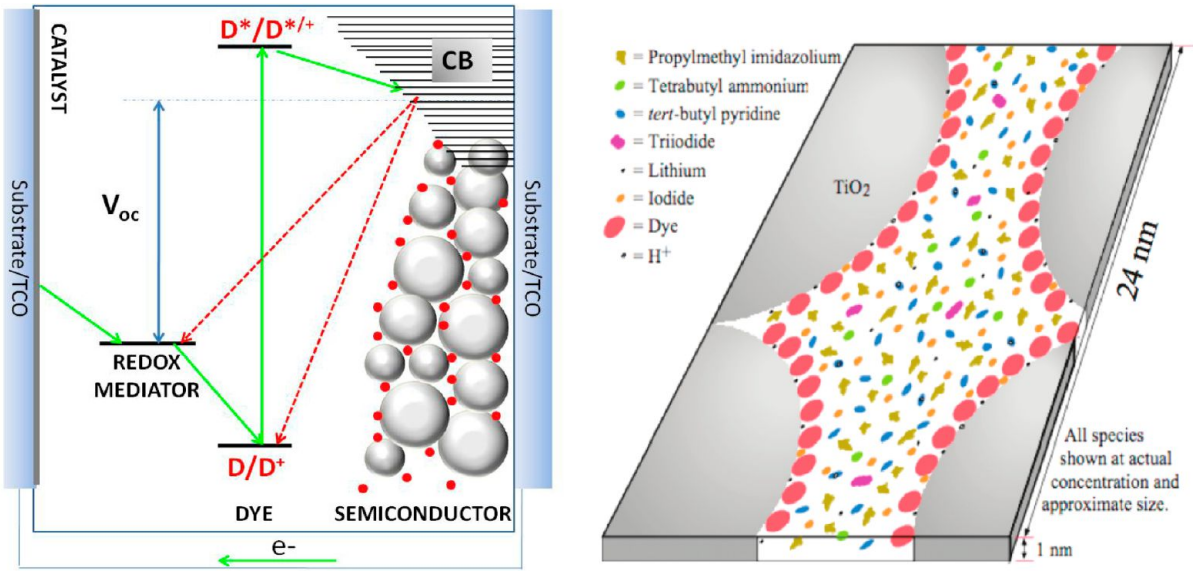

[a]Green lines correspond to forward electron-transfer steps, and red lines correspond to parasitic recombination reactions.

[b]Reprinted from ref 42.

coefficient or peculiar supramolecular interactions compared to those of N719 or N749, thus enhancing the DSCs' overall stability and/or efficiency.[10−14] Fully organic sensitizers have been developed as metal-free dyes because of their increased molar extinction coefficient, compared to Ru(II) dyes, spectral tunability, and reduced environmental impact.[15,16] When employing the most common I^-/I_3^- redox shuttle, organic dyes have delivered very high photovoltaic efficiencies, exceeding 10%.[17] Functionalized donor−acceptor Zn(II) porphyrins have recently emerged as a new class of sensitizers with high performance potential due to the extended absorption spectrum in the red, up to the near-IR (NIR) region.[18−20] Most of current research on dye sensitizers has been focused on enhancing the dye spectral response, either in terms of stronger and/or more extended absorption, although both requisites are usually difficult to get within a single molecule. An appealing strategy to overcome the limits of a single dye was the employment of dye cocktails or of cosensitization strategies, whereby different dyes are used to absorb different portions of the solar spectrum.[21−35] As a matter of fact, the new DSCs' efficiency record, close to 13%, was obtained by the combination of a Zn(II) porphyrin and an organic dye, showing complementary absorption.[20]

TiO_2 is established as the most performing semiconductor metal oxide in DSCs, both in the form of the commonly employed sintered nanoparticles and nanotubes/nanorods;[36,37] alternative metal oxides to TiO_2, such as ZnO and SnO_2, are also actively investigated.[38−41]

The standard redox shuttle in DSCs is the I^-/I_3^- redox couple in a volatile organic solvent (typically acetonitrile),[6,9] even if the field has very recently been revolutionized by Co(II)/Co(III) redox couples, which allowed for demonstration of photovoltaic efficiency close to 13%.[20]

The DSC is an inherent complex system because, in most cases, the interdependencies among the various components dictate the overall device performance. A schematic representation of a 1 nm slab sliced from a pore in a DSC made by the N719 dye in contact with an iodine-based electrolyte of typical composition is reported in Scheme 1, from ref 42.

As can be noticed, the ideal optimization of the individual DSC components is very hardly mapped into the realistic picture of Scheme 1, whereby strong interdependencies are likely to occur. Relevant pair interactions include, but are possibly not limited to, (i) dye−semiconductor, (ii) redox shuttle−semiconductor, (iii) dye−redox shuttle, and (iv) dye−dye and dye−coadorbent interactions.

Dye−Semiconductor Interactions. The interaction between the sensitizing dye and the semiconductor is related to the primary charge generation event in DSCs, that is, the dissociation of the dye molecular exciton leading to electron injection from the dye excited state into the manifold of semiconductor CB states. A salient feature of efficient dyes is indeed the presence of suitable functional groups able to strongly bind to the semiconducting oxide surface. The anchoring group should coincide with, or be very close to, the dye acceptor moiety, where unoccupied electronic states are spatially confined. This promotes electronic coupling between the donor levels of the excited dye and the delocalized acceptor levels of the semiconductor CB and helps the charge injection process.[43−45]

The sensitizer's anchoring group should also provide stable grafting of the dye onto the semiconductor surface, thus leading to long-term device stability.[46−48]

When a dye binds to a semiconductor surface, two main interactions might be at work from the semiconductor side, (a) an electrostatic effect, mainly due to the dye dipole moment, and (b) the effect of the charge transfer (CT) between the dye and the semiconductor, which may accompany the dye−semiconductor bond formation. Both effects can alter the position of the semiconductor CB and therefore influence the DSCs' functioning.[49] Also, upon binding to the semiconductor, some of the dye protons, carried by the acidic carboxylic groups, can be transferred to the surface, charging it positively, thereby leading to CB energy shifts. From the dye side, apart from the aforementioned dissociation of the acidic carboxylic

dx.doi.org/10.1021/jz302147v | J. Phys. Chem. Lett. 2013, 4, 956−974

group, the main effect is the broadening of the dye excited states, which is related to electron injection rate.[43,50−52]

Redox Shuttle−Semiconductor Interactions. The main redox shuttle−semiconductor interactions relevant in DSCs are those related to the presence of potential-determining ions in the electrolyte solution (e.g., Li^+).[53,54] Also, the nature of the electrolyte solvent might directly or indirectly (e.g., by the solvent acid/base chemistry) affect the semiconductor properties. TiO_2 is known to exhibit a Nernstian response to variations in pH, which leads to a 0.059 V positive shift (versus NHE) of the CB energy per pH unit decrease. A similar positive shift occurs by interaction of Li^+ ions with TiO_2.[55−57] These positive CB shifts lead to increased DSC photocurrents but reduced open-circuit voltages, so that usually some compromise solution is adopted. Also, the electrolyte solvent can interact with the semiconductor and lead to CB shifts, although these are most likely an indirect manifestation of the aforementioned pH-induced shift due to the proticity or hydration of various solvents.[53,54,58,59]

Dye−Redox Shuttle Interactions. Dye−-redox shuttle interactions have been invoked in many instances to explain the correlation between structural/chemical dye variations and their functioning in DSC devices. In particular, some authors[60−65] suggested the idea that particular atoms or chemical groups can provide binding sites for I_2 (I_3^-), increasing its concentration close to the TiO_2 surface and thus accelerating the recombination and/or dye regeneration processes. O'Regan et al.[60] found that the replacement in the ligands of a ruthenium dye of two oxygen atoms with two sulfur atoms caused a 2-fold increase in the recombination rate and, on the basis of literature data, ascribed such a difference to a stronger tendency of ethylthioether compared to ethylether to bind I_2. Very recently, the same authors measured the binding coefficients for iodine and ruthenium dyes and related this observations to recombination processes in DSCs.[66] An extensive investigation on the effects of dye molecular structure and electrolyte composition on the recombination dynamics has been reported by Miyashita et al.,[61] who examined the photovoltaic performances of a series of organic- and ruthenium-dye-based DSCs, consistently finding lower electron lifetime values for the metal-free-based DSCs compared to those employing ruthenium dyes. This was interpreted as arising from an increased I_3^- concentration in the proximity of the oxide surface, yielding higher recombination rates. Recently, Mosconi et al.[67] reported on the interaction between Co(III) ions in the redox shuttle and the anionic N719 dye, which led to a strong efficiency loss due to enhanced recombination.

Dye−Dye and Dye−Coadsorbents Interactions. Dye sensitizers give dense packing on the titania surface, usually described as surface monolayers,[68−72] although in some cases, dye multilayers have been detected.[73] The dye surface coverage can substantially vary depending on the molecular structure of the dye and the dyeing conditions (e.g., solvent, dipping time, use of coadsorbents, etc.). Typical D−π−A organic dyes characterized by a cyanoacrylic anchoring group, such as C218, JK2, Y123 or D35, just to cite a few examples, usually show high surface coverage, which has been reported to be in the range of ∼2 molecules per nm^2.[68,69] This coverage value is suggestive of dense dye packing; this is in turn related to the dyes typically lying almost perpendicular to the TiO_2 surface, as revealed by photoelectron spectroscopy (PES)[74] and by computational modeling studies.[75,76]

For D−π−A organic dyes featuring a rhodanine-3-acetic acid anchoring group, on the other hand, lower surface coverages in the range of 0.3−0.6 molecules per nm^2 have been reported.[70] This is most likely due to the different dye binding mode related to the different anchoring,[75,77] which results in the dye lying almost parallel or with an angle of ∼45° with respect to the TiO_2 surface. This adsorption mode, which is peculiar of indoline dyes, such as D102 and D149, is characterized by strong π-stacking interactions, which are manifested by fast hole transfer among surface-adsorbed dyes.[78]

Ruthenium dyes, such as the prototypical N3 or N719, N749, and C101 dyes, show surface coverages in the range of 0.3−0.8 molecules per nm^2,[71,73] although values as high as 1.8 molecule/nm^2 have been reported upon formation of dye multilayers.[73] For the Z907 dye, featuring nonyl alkyl chains on the ancillary bipyridine ligand, and for the related dye with methyl instead of nonyl substituents, the close packing upon TiO_2 adsorption was found to result in very high hole diffusion rates, which were not manifested by the N3 dye.[79] This was related to the sizable intermolecular interactions occurring for surface-adsorbed dyes, which for Z907 led to a close proximity of the NCS ligands, where the HOMO is partly localized.[79,80] Intermolecular interactions between surface-adsorbed dyes were also found to lead to different PES spectra for N3 and N719 dyes, with computational analyses pointing at hydrogen bonding as being responsible for the differently observed behavior.[81,82] It is also interesting to notice that for ruthenium dyes, varying surface coverages have been reported for TiO_2 exhibiting mainly (001) or (101) surfaces,[83] the latter corresponding to the most abundant surface in anatase TiO_2. This different behavior was related by computational modeling studies to the different dye adsorption modes on the two surfaces.[71]

Dye−dye intermolecular interactions are of paramount importance in determining the overall DSC conversion efficiency because they significantly affect the charge generation (a higher dye loading absorbs more light) and may inhibit the parasitic recombination reactions between TiO_2-injected electrons and oxidized species in the redox shuttle; a compact dye monolayer would act as an insulating layer toward the approach of the electrolyte to the TiO_2 surface. The formation of a homogeneous (partial) dye layer was recently shown to be critical for DSC performances.[84]

The strong dye−dye intermolecular interactions, which contribute to determine the compactness of the dye layer, have however the drawback of introducing undesired effects that may limit the DSCs efficiency. These include a filtering effect by non-TiO_2-adsorbed dye molecules, possibly found as a dye overlayer, which would absorb light but not produce photocurrent. Also, dye aggregation is known to lead to intermolecular excited-state quenching, reducing the DSCs photocurrent.[85−87] Dye aggregation is usually manifested by a marked broadening of the absorption spectrum upon TiO_2 adsorption compared to dyes in solution; see Figure 1 for the typical example of indoline dyes. In some limited cases, however, a controlled aggregation has been proven to enhance the photocurrent generation as a result of the larger light absorption window of the aggregates, possibly combined to an efficient CT from the aggregate excited state to the semiconductor.[86,88−90]

An appropriate molecular design and the use of antiaggregation coadsorbents can prevent in some measure the dye aggregation on the TiO_2 surface, improving the overall

dx.doi.org/10.1021/jz302147v | J. Phys. Chem. Lett. 2013, 4, 956−974

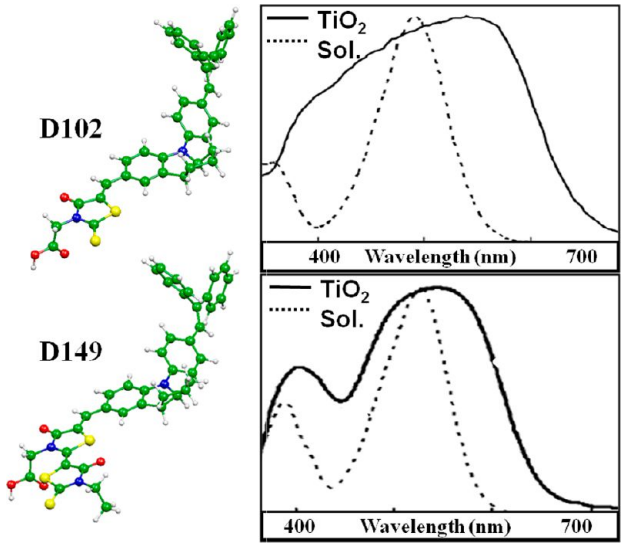

Figure 1. Molecular structures and absorption spectra of two prototypical indoline dyes, namely, D102 (upper right) and D149 (lower right), in solution (dashed line) and on TiO_2 (solid line). Adapted from ref 77.

photovoltaic performances.[89] One of the most employed coadsorbates is chenodeoxycholic acid (CDCA),[91,92] which competes with the sensitizer in the adsorption process on the titania surface; more recently, other coadsorbates, yielding to notably improved cell performances, have also been reported.[9,93,94] The major benefits coming from the use of CDCA, or similar coadsorbents, are thought to be related to (i) filling the vacancies in the dye-sensitized TiO_2 film in such a way to reduce the charge recombination of electrons in the TiO_2 with the redox shuttle (blocking effect)[95] and (ii) reducing intermolecular quenching phenomena;[85−87,96,97] some authors also reported effects of CDCA on the TiO_2 CB, leading to increased open-circuit voltages.[98]

Dye−dye intermolecular interactions are fundamental in determining the fate of cosensitized DSCs, in which two different dyes have to be accommodated on the TiO_2 surface in an optimal ratio.[20,21,27,30,99,100] Despite the great potential of cosensitization to achieve a panchromatic light harvesting, only in a few cases have significant efficiency improvements been obtained,[20,26,33,35] mainly due to energy or electron/hole transfer between coadsorbed dyes or because of modulation of the charge-recombination behavior. An appealing strategy to achieve high cosensitized DSC efficiency has been recently reported, whereby spatially isolated chromophores are selectively positioned in desired zones of the photoanode.[101] An interesting alternative to traditional cosensitization, in which both chromophores may inject electrons into TiO_2, is the use of energy relay dyes (ERD), which may transfer the excitation energy to a sensitizing dye (SD) by virtue of energy transfer (either by Förster or Dexter mechanisms).[100,102,103] For the case of fluorescence (Föster) resonance energy transfer (FRET),[104] the ERD has to remain electronically insulated from the TiO_2 surface and solely transfer its excited-state energy to the SD to produce additional photocurrent.[103] The geometry of the ERD donor−SD acceptor system is crucial to determine the energy-transfer rate and contributes to determining the Föster radius (defined as the distance between the donor and the acceptor when the FRET has 50% probability[103]) by the orientation factor κ^2.[105] It is obvious that the cosensitization pattern and thus the ensuing DSCs efficiency strictly depend on the intermolecular interactions among the FRET partners.

Computational Tools. Theoretical modeling of isolated cell components (e.g., dye, semiconductor nanoparticles, redox shuttle, and so forth) as well as of combined dye−semiconductor−redox shuttle systems[106,107] can successfully assist experimental research by providing in silico design of new sensitizers and a deeper comprehension of the basic chemical physics processes governing the cell functioning and its performances. A computational approach to DSC modeling can be essentially casted into a stepwise problem, whereby one first needs to accurately simulate the individual DSC components to move to the relevant pair (or higher-order) interactions discussed above. This information might then constitute the basis for an integrated multiscale computational description of the device functioning, which may further boost the DSCs' efficiency along with providing the basic understanding of the device necessary for further enhancing target DSC characteristics, such as temporal stability and optimization of device components.

A computational approach to DSC modeling can be essentially casted into a stepwise problem, whereby one first needs to accurately simulate the individual DSC components to move to the relevant pair (or higher-order) interactions.

Here, we present a unified view of our recent activity on the computational modeling of relevant intermolecular interactions occurring in DSCs. If not otherwise stated, we review previously published results from our laboratory, which are integrated by new calculations to offer a critical view of the field. In particular, after briefly describing the methodological aspects underlying the computational description of intermolecular forces, we concisely review the adsorption of isolated organic and ruthenium dyes on TiO_2. We then move to the focus of the present work, which is the description of multiple-dye adsorption on TiO_2 relevant to aggregate properties and the simulation of cosensitized patterns involving both different dyes and dye−coadsorbent interactions.

Modern first-principles computational methodologies, such as those based on density functional theory (DFT) and its time-dependent extension (TDDFT), provide the theoretical/computational framework to describe most of the desired properties of the individual dye−semiconductor systems and their interface. These methods, however, usually substantially fail in reproducing weak intermolecular interactions, which require the accurate treatment of dispersion forces (often referred to as van der Waals forces), arising from fine long-range electron correlation effects.[108−111] In ab initio wave-function-based approaches, correlated methods are necessary to recover the dispersion energy; usually, the second-order Møller−Plesset perturbation (MP2) and coupled-cluster methods deliver accurate interaction energies for weakly bound systems but present slow convergence with respect to the number of basis functions and (highly) unfavorable scaling

dx.doi.org/10.1021/jz302147v | J. Phys. Chem. Lett. 2013, 4, 956−974

of the computational cost as the system size increases. All standard DFT methods yield repulsive interactions between dispersion-bound adducts rather than the $1/R^6$ behavior typical of dispersion attraction, where R is the interatomic distance. The development of DFT-based methods that accurately account for weak intermolecular interactions is becoming one of the most active research lines in computational chemistry, physics, and materials science.[112] Various meta-generalized gradient approximation DFTs, expressly parametrized to give better van der Waals binding energies, have been recently developed and implemented in the mostly used quantum chemistry codes, the M05, M05-2X, M06, and M06-2X functionals.[113−115] An alternative and simpler approach, known as the DFT-D method, is to correct the DFT energy by adding an empirical potential of the form C_6R^{-6}, where C_6 are the dispersion coefficients; in the framework of DFT-D methods, various strategies have been developed to obtain the empirical dispersion coefficients.[116−122] When the interaction energies of more than two dye sensitzers (dimer) need to be evaluated, MP2 calculations become rapidly unfeasible, and one needs to resort to DFT-based approachs, such as the D3 correction by Grimme and co-workers,[120,123] which has been shown to provide reliable results.[63,105] For computational details, employed program packages, and models, we refer the reader to the Supporting Information, which reports the technical details for the cases presented in the following.

Single-Dye Binding to TiO_2: Organic and Ruthenium Dyes. As a prerequisite to investigate intermolecular interactions occurring among surface-adsorbed species, one needs to simulate the adsorption mode of a single adsorbent on TiO_2, which is thus briefly reviewed here. The anchoring mechanism of the largely employed carboxylic acid group onto the semiconductor surface can be exemplified by referring to the coordination modes of the carboxylate fragment (COO^-) to metal ions; there are basically three possible coordination modes, that is, monodentate, chelated, and bridged bidentate.[124,125] Computational modeling has significantly contributed to a better understanding of the intimate dye−semiconductor interactions characterizing the crucial DSCs' heterointerface.[126,127] A number of theoretical studies on the dye adsorption modes on the TiO_2 surface have been published,[75−77,107,128−141] starting from the pivotal work by Vittadini et al. on the formic acid adsorption on the TiO_2 anatase (101) surface.[142] The calculations show that for the organic dyes bearing a carboxylic acid as the anchoring group, the preferred adsorption mode is bidentate bridging, with one proton transferred to a nearby surface oxygen,[77,134,143,144] while the monodentate anchoring is usually predicted to be less stable, although some dependency of the relative stability of these two anchoring modes on the employed computational methodology can be outlined.[76,142,145] Recently, we reported a combined FT-IR and computational investigation on acetic acid adsorption on TiO_2 as a probe of the adsorption of the most employed carboxylic anchoring group.[76] Our results pointed at the bridged bidentate adsorption as the most likely anchoring mode, based on both energetics considerations and the similarity of the calculated and experimental IR spectra.

As depicted in the left panel of Figure 2, the two most employed anchoring groups in organic sensitizers, that is, cyanoacrylic acid and rhodanine-3-acetic acid, yield rather different orientations of the molecules with respect to the oxide surface when bound in the bridged bidentate mode; the molecule is perpendicular to the surface in the case of the cyanoacrylic group (a), whereas it lies almost flat when the rhodanine anchoring group is considered (b).[75]

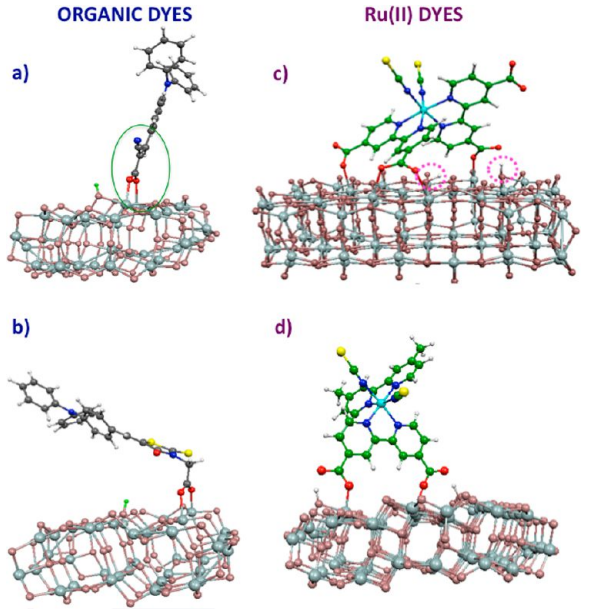

Figure 2. (Left panel) Equilibrium adsorption geometries, in the bidentate bridging mode, of two representative organic dyes bearing (a) cyanoacrylic acid and (b) rhodanine-3-acetic acid anchoring groups. (Right panel) Adsorption geometries of two prototypical Ru(II) complexes, (c) N719 with three anchoring groups (one bidentate bridging and two monodentate) and (d) Z907 with a methyl instead of nonyl substituent with two monodentate anchoring units.

The situation is more complicated in the case of typical ruthenium dyes, for which two to four carboxylic functions are present on the same dye. While heteroleptic dyes, carrying one carboxy-substituted bipyridine, are usually found to bind to TiO_2 by both carboxylic groups[71,105] (see Figure 2d), similar to that found for the bare bipyridine ligand,[146] for the prototypical N719 dye, adsorption by up to three carboxylic groups was found to be viable.[132,147] For the related black dye, carrying a carboxy-substituted terpyridine ligand, various anchoring modes were reported, depending on the protonation of the dye,[148] similar to that found for the N719 dye.[132]

Multiple-Dye Adsorption on TiO_2: Dye Aggregation and Aggregate Properties. Taking as a starting point the optimized geometry of a single dye molecule adsorbed on TiO_2, one can try to model the dye packing on the surface by employing a simple topological approach and assuming that in the sensitization process, the dye−TiO_2 interactions, which results from the chemical bonds between the dye anchoring groups and the semiconductor surface, are stronger that the intermolecular ones, thus guiding the formation of the dye monolayer.[62,77,105] The dye molecular structure, on the other hand, reflects the peculiar dye−dye interactions, which determine the energetically favored aggregation motifs among all of the possible ones. In other words, we assume that the five-coordinated Ti atoms on the surface dictate the possible adsorption sites, the dye−surface interactions govern the binding mode and the adsorption geometry, and the interactions among adsorbed dye molecules give the tendency to form a particular aggregation pattern. This assumption is grounded in the observation that dye−TiO_2 binding energies are usually ∼3 times larger[149] than intermolecular interaction energies for highly interacting organic dyes.[77]

dx.doi.org/10.1021/jz302147v | J. Phys. Chem. Lett. 2013, 4, 956−974

Organic Dyes. To model the formation of possible aggregates of two indoline dyes, termed D102[96] and D149,[150] and to investigate the relation existing between the molecular structure of the dye and its tendency to form aggregates on the TiO_2 surface (Figure 1), we employed a TiO_2 nanoparticle model consisting of a (101) $(TiO_2)_{82}$ anatase slab of approximately 4 nm^2 area, with three rows of five- and six-coordinated surface Ti sites and sufficient coordination sites to accommodate the considered dimeric arrangements (see section S1.4 in the Supporting Information for further computational and model details).

Table 1 lists the MP2 and B3LYP relative energies of the deprotonated dimers at their adsorption geometry on TiO_2,

Table 1. B3LYP and MP2 Relative Energies (kcal/mol) of a Series of Dimers of D149 and D102 Extracted from the Corresponding Optimized Geometries on TiO_2[a]

	D102		D149	
dimer	B3LYP	MP2	B3LYP	MP2
(0,2)	6.80	0.00	12.49	4.50
(2,2)	5.57	3.94	3.23	0.00
(4,2)	0.00	4.47	0.00	3.62
(−2,2)	4.14	4.81		
(4,0)	10.03	1.64		
(−1,1)	11.23	1.23		

[a]The nomenclature (*x*,*y*) adopted to indicate the position of the second molecule on the TiO_2 surface is illustrated for the two most stable cases in Figure 3, in ref 77, and in the Supporting Information.

calculated in ethanol solution with reference to the most stable configuration (the nomenclature is illustrated in Supporting Information, Figure S1). An interesting picture comes out from MP2 results; the lowest-energy configuration for D102 is that termed (0,2), having the two molecules aligned along the *y* direction with the π systems almost perfectly stacked, Figure 3. Most notably, this arrangement turns out to be the highest in energy for D149 (by 4.5 kcal/mol), while the preferred configuration is (2,2), with the molecules separated by one Ti atom along the *x* axis, Figure 3. It is also worthwhile to notice that for D102, there are at least two other arrangements, namely, (4,0) and (−1,1), precluded to D149 because of the presence of the second rhodanine ring, which are very close in energy to the (0,2) dimer. As is also apparent, the energetics obtained by DFT and MP2 are rather different. For both dyes, DFT does not predict dye aggregation, delivering an increasing stability as the distance between the two dye molecules increases; the (4,2) configuration is predicted to be the more stable one for both D102 and D149.

Because MP2 calculations can easily become very computationally expensive as the number of atoms and basis set dimensions increase, we have benchmarked the more computationally affordable B3LYP-D3 method against B3LYP and MP2 methods for the favored (2,0)-D102 and (2,2)-D149 dimers. The results are in this case obtained in vacuo for the protonated dyes at their optimized adsorption mode on TiO_2. The results, reported in Table 2, show a similar description of the interchromophore interaction by B3LYP-D3 and MP2 methods (a rigid increase of the interaction energy by ∼2 kcal/mol is found by B3LYP-D3 compared to MP2), while B3LYP does not predict any binding between the two monomers. Also in line with our previous results, the (0,2)-D102 dimeric arrangement is substantially favored compared to the (2,2)-

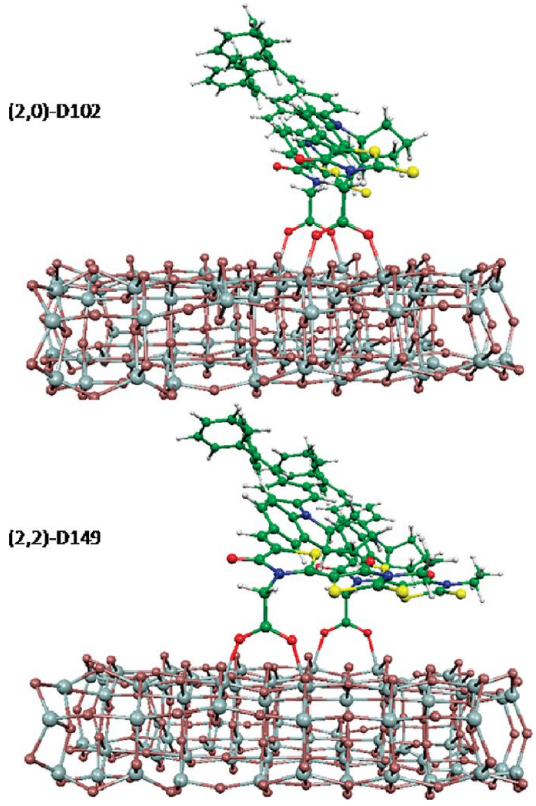

Figure 3. Optimized structures of the preferred (0,2)-D102 (top) and (2,2)-D149 (bottom) configurations. Reprinted from ref 77.

Table 2. B3LYP, B3LYP-D3 and MP2 Interaction Energies (kcal/mol) for the Most Stable D102 and D149 Dimeric Arrangements of Figure 3

System	B3LYP	B3LYP-D3	MP2
(0,2)-D102	−0.10	−16.27	−14.08
(2,2)-D149	+1.42	−10.02	−8.04

D149 case, with ∼6 kcal/mol higher interaction energies, testifying the larger tendency of the D102 dye to form aggregates. As expected, lower interaction energies are calculated in solution for the deprotonated dyes, which, for the D102 case, amount to 9.0 kcal/mol. As a further check of our computational protocol and to quantify the effect of the basis set quality on the calculated energies, for the (0,2)-D102 dimer, we carried out new calculations with a 6-311++G** basis set, finding a B3LYP-calculated interaction energy of −0.9 kcal/mol to be compared to the −0.1 kcal/mol obtained with the 6-31G* basis. This minimal difference justifies the use of the more computationally convenient 6-31G* basis set.

On the basis of the stability order discussed above, we report in Table 3 the excitation energies and the oscillator strengths of the lowest excited states for the relevant dimeric configurations (0,2), (4,0), and (−1,1) for D102 and (2,2) for D149. The energy shifts are computed with respect to the lowest excited states of the standalone D102 and D149 dyes.

The results show that the different aggregation schemes investigated for D102 have different, and even opposite, effects on the excited states. In fact, the (4,0) configuration with the molecules placed side-by-side and the π-systems almost parallel produces a blue shift of the excited states, typical of so-called H-aggregates. If one looks at the excited state with the largest

dx.doi.org/10.1021/jz302147v | J. Phys. Chem. Lett. 2013, 4, 956−974

Table 3. Computed Excitation Energies (eV) and Oscillator Strengths for the D102 and D49 Reference Monomer and for the Most Stable Dimers of D102 and D149[a]

monomer	exc.	f	composition	dimer	exc.	f	shift
D102	2.11	0.820	H → L 90%	(0,2)-D102	1.96	0.022	−0.15
					2.10	1.016	
					2.18	0.537	
					2.28	0.001	
				(4,0)-D102	2.13	0.075	+0.02
					2.14	0.077	
					2.21	1.195	
					2.27	0.048	
				(−1,1)-D102	2.00	0.028	−0.11
					2.09	0.535	
					2.23	0.698	
					2.30	0.283	
D149	2.05	0.805	H → L 92%	(2,2)-D149	1.97	0.007	−0.08
					2.05	0.720	
					2.07	0.784	
					2.23	0.001	

[a]The corresponding shifts (eV) with respect to the reference monomers are listed in the last column.

oscillator strength (1.195), located at 2.21 eV, the blue shift of the absorption maximum for the (4,0) dimer is even more pronounced, amounting to ∼0.1 eV, so that this aggregation pattern can be reasonably disregarded. On the other hand, the two D102 dimeric arrangements, which induce a sizable $\pi-\pi$ stacking, (0,2) and (−1,1), imply the appearance of new bands in the absorption spectra that are substantially red shifted compared to the monomer spectrum (0.15 and 0.11 eV, to be compared to a 0.23 eV experimental shift), a characteristic signature of J-aggregates. Notably, the most stable (0,2)-D102 dimer shows also the largest red shift. If we now compare the calculated data for D102 and D149, this model almost quantitatively reproduces the different spectroscopic behavior of the two dyes adsorbed on the TiO_2 surface. Selecting the most stable configurations, the red shifts computed upon aggregation are 0.15 and 0.08 eV for D102 and D149, respectively, to be compared to the experimentally measured values of 0.23[96] and 0.07 eV.[150] Most notably, also the computed oscillator strengths for the dimer excited states further reveal a stronger interaction in the case of the (0,2)-D102 configuration, with a ∼3-fold reduction of the J-band oscillator strength calculated in (2,2)-D149. Overall, the larger shift and higher intensity of the new spectroscopic feature appearing in D102 as a function of dye aggregation is perfectly in line with the available experimental information.

Having modeled the dye adsorption and the formation of surface aggregates, in principle, one possesses a realistic model to investigate and reproduce a series of interfacial phenomena that are strictly related to the dye packing on the TiO_2 surface, such as, for instance, the occurrence of spectral shifts on the ground-state absorption spectrum of the semiconductor-adsorbed dyes.[144,151−158] These effects manifest themselves as absorbance changes occurring for the neutral adsorbed dyes, which have been detected by both transient absorption and PIA spectroscopy. Various interpretations have been adduced to explain the observed band shifts and intensity changes. Staniszewski et al.[154] attributed the spectral changes to a marked change occurring in the dye environment after electron injection and regeneration by iodide, essentially due to slow cation transfer; basically, electron injection perturbs the electrostatic environment surrounding the dye, which slowly responds by displacing positive charges due to solution or surface-adsorbed Li^+ ions or protons. The appearance of similar or related peak bleaches in the adsorbed dye absorption spectrum has also been ascribed to possible phenomena of electron accumulation into the semiconductor, affecting the LUMO of the dye[156] or electron extraction[157] from the TiO_2, as well as to the presence of long-lived photoreduced dye molecules.[155] However, more recently, some authors argued[151−153] that the measured spectral changes are consistent with first-order transient Stark effects.[159−161] Such local electric fields, which show maximum amplitude at the initial observation times after electron injection, are expected to be associated with the electron transfer from the dye to the TiO_2 film and to the consequential formation of oxidized dye molecules.

Exploiting the work on the aggregation of the indoline dyes and employing a model that "statically" simulates the oxidation/electron injection and regeneration steps and the associated optical responses, we provided a computational framework to interpret the Stark shifts experimentally observed by Cappel and co-workers for D149-sensitized solar cells (see section S1.4 in the Supporting Information for computational details).[153] Figure 4 shows a schematic representation of the model employed to simulate the Stark shifts along with the representative calculated electronic structures. The different cases examined here are (i) left side, the neutral dye dimer, hereafter labeled N/TiO_2(0), with its two quasi-degenerate intramolecular CT (ICT) transitions, HOMO → LUMO + 1 and HOMO − 1 → LUMO and (ii) right side, the cationic system originating from the removal of one electron from the dye dimer, with the charge hole mainly localized on the left monomer (sum of Mulliken charges = 0.97 e) and the HOMO → LUMO excitation occurring in the neutral dye (sum of Mulliken charges = 0.03 e) on the right side in the presence of the charge hole on the left side dye. Using this cationic dimer, indicated as C/TiO_2(0), one can thus evaluate how the presence of the positive charge, mainly localized on one dye molecule, perturbs the absorption spectrum of the adjacent dye. As a further expansion of our model, we also simulated the case of an electron injected from the dye to the semiconductor CB, C/TiO_2(1), so that the cooperative effect of the dye cation and

dx.doi.org/10.1021/jz302147v | J. Phys. Chem. Lett. 2013, 4, 956−974

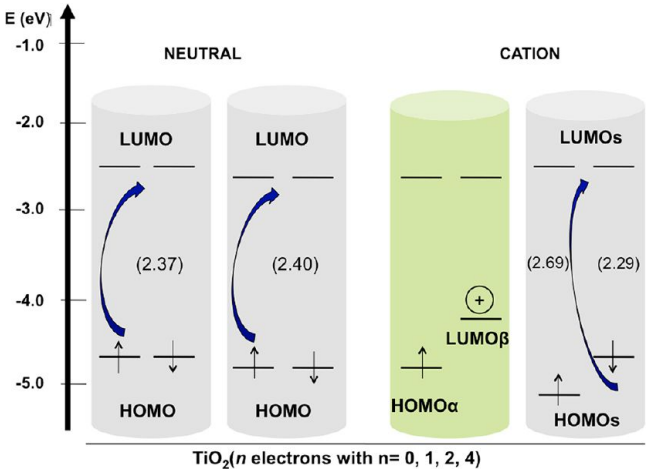

Figure 4. Schematic representation of the electronic structure of the neutral and cationic model systems employed, with the corresponding HOMO−LUMO gaps calculated at the B3LYP/6-31G* level in acetonitrile solution reported within parentheses. The following cases are examined: N/TiO_2(n) with n = 0, 1, 2, and 4 and C/TiO_2(n) with n = 0 and 1; see the text for definitions.

of the charge in the TiO_2 can be accounted for. This is a simple yet effective method to account for the injected charge into the semiconductor, which can be coupled to excited-state TDDFT calculations. Finally, as hypothesized by Cappel et al.[156] and Anderson et al.,[157] local accumulation or depletion of electronic charge into the TiO_2 nanoparticles could also affect in some measure the spectroscopic properties of the absorbed sensitizers, yielding the measured spectral shifts. We, hence, examine here the effect on the absorption spectrum of the neutral dimeric system arising from an incremental "local" charge accumulation in the oxide CB, considering the cases of N/TiO_2(n), with n = 1, 2, and 4.

For the deprotonated N/TiO_2(0) dimer in acetonitrile, we calculated two intense quasi-degenerate transitions at 2.07 and 2.09 eV, with oscillator strengths of 0.76 and 0.83, respectively, which essentially correspond to the ICT excitation of the two monomers. If the electronic coupling between the two molecules is weak, as is the case for (2,2)-D149,[77] upon extraction of one electron, the hole can be localized on a single dye molecule, yielding the cationic dimer schematically represented on the right side of Figure 4 and whose frontier molecular orbitals are displayed in Figure 5 (left side). In line with experimental evidence,[153] the calculated absorption spectra plotted in Figure 5 (right side) clearly show that for all of the examined model cases, a blue shift in the absorption, even if of different magnitude, is predicted. Interestingly, what is apparent from our results is that taken alone, the effect of the injected electrons into the TiO_2 is rather small,[144] and the injected charge seems to be only in part responsible for the sizable observed spectral changes. In fact, when the presence of the adjacent oxidized molecule is taken into account, the computed absorption blue shift is remarkable, and such optical response is consistent with the appreciable Stark shifts

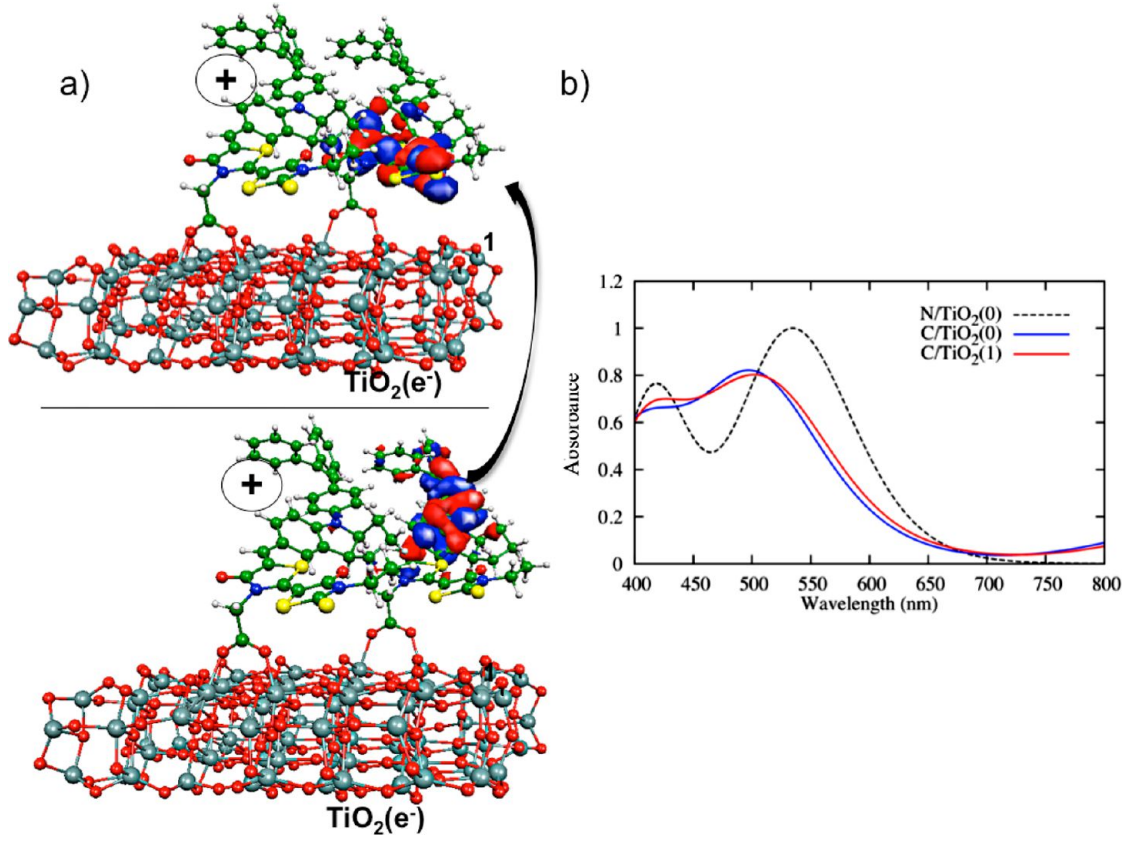

Figure 5. (Left) Isodensity surface plots of the frontier molecular orbitals for the (2,2)-D149 cationic dimer calculated at the B3LYP/6-31G* level in acetonitrile. (Right) Absorption spectra in acetonitrile solution of (2,2)-D149 for the N/TiO_2(0), C/TiO_2(0), and C/TiO_2(1) cases, simulated by a Gaussian broadening with σ = 0.20 eV and normalized to the N/TiO_2(0) maximum intensity. The spectra have been shifted by 0.28 eV to make the experimental maximum of D149 and the calculated excitation coincident.

dx.doi.org/10.1021/jz302147v | J. Phys. Chem. Lett. 2013, 4, 956−974

experimentally measured.[153] The absorption maximum moves from 526 to 494 nm, with a shift of 0.15 eV, in the case of the $C/TiO_2(1)$ system and to 489 nm, with a shift of 0.18 eV, for $C/TiO_2(0)$.

The presented model, therefore, nicely accounts for the experimentally observed band shifts and, more importantly, indicates that the effect of positive charge localized on adjacent dyes seems to play a sizable role in blue shifting the absorption spectrum of neutral dyes, as a consequence of the strong intermolecular electrostatic interaction. In this respect, we speculate that the aggregation pattern of the dyes and their tendency to form highly packed layers might influence to some extent the magnitude of the Stark shift.

To conclude the section devoted to the aggregation of organic dyes on the titania surface, we shall show, by discussing the case of the donor−acceptor p-conjugated organic dye (termed MP124 and depicted in the left side of Figure 6)

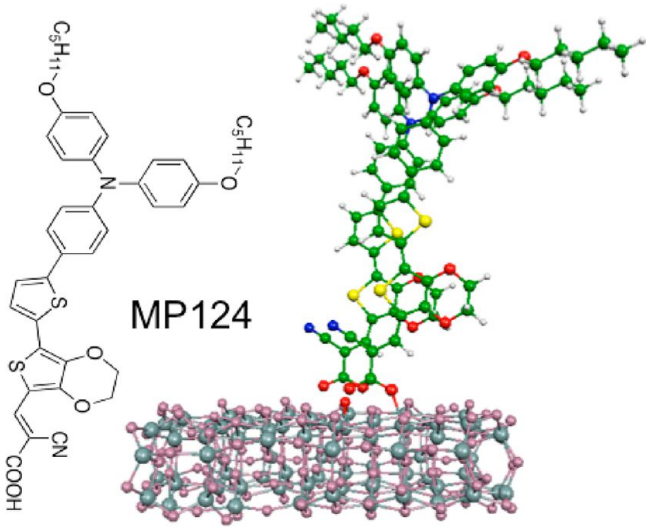

Figure 6. Chemical structure of the MP124 dye (left) and optimized molecular structures of the preferred dimeric arrangements of MP124, termed (−1,1) (right).

reported by Planells et al.[62] that an appropriate molecular design, with the introduction of bulky groups, can effectively prevent aggregation phenomena. The DFTB-optimized structure of the most stable dimeric configuration, termed (−1,1), which guarantees the weaker interaction among the O−R chains, is reported in Figure 6. Interestingly, for the most stable dimer, the MP calculated interaction energy, amounting to 1.3 kcal/mol, is smaller than that reported above for the indoline dimers. Despite the different geometry optimization level, these data suggest a smaller tendency of this class of dyes to form close aggregates on the oxide surface. This is confirmed by the similarity of the absorption spectrum in solution and upon TiO_2 adsorption found for this type of dye;[62] see Figure 7. Our data are consistent with the binding energies calculated by O'Rourke and Bowler for isolated tetrahydroquinoline and carbazole dyes (similar to the MP124 dye discussed above) on TiO_2 and for the corresponding data for adsorption of dye a monolayer, which showed a preference for adsorption of the isolated dyes.[162]

Ruthenium Dyes. To the best of our knowledge, the aggregation of ruthenium dyes on TiO_2 has never been computationally investigated beyond the work of Patrick et al. on the hydrogen bonding of TiO_2-adsorbed N3.[81] Here, we report preliminary unpublished results obtained for the heteroleptic Z907 dye with nonyl chains replaced by methyl groups, which was investigated by Wang et al. in ref 79. We report in Figure 8 the DFT-optimized geometry of a TiO_2-adsorbed ruthenium dye dimer (computational details in section S1.4 in the Supporting Information).

The two dyes were considered to be adsorbed on the same two rows of Ti atoms, which ensures a close interaction distance, avoiding explicit atomic superimposition. Although this interaction geometry might not be the most stable dimeric arrangement, this is a useful model to provide an estimate of the strength of intermolecular interactions for this type of dyes. We also notice that this adsorption mode corresponds to a surface coverage of ∼0.5 dye molecules/nm^2, which is quite typical for this class of ruthenium dyes.[71,73]

For the ruthenium dye dimer reported in Figure 8, we calculated a B3LYP-D3 interaction energy in vacuo of 9.0 kcal/mol, which is smaller than the 16.3 kcal/mol value computed for the D102 organic dye at the same level of theory; see Table 2. As an estimate of the electronic coupling occurring between the two TiO_2-adsorbed dyes, we evaluated by DFT (B3LYP/3-21G*) the dye-based HOMO splitting for the surface-adsorbed dimer, finding a value of 0.01 eV and thus a coupling of 0.005

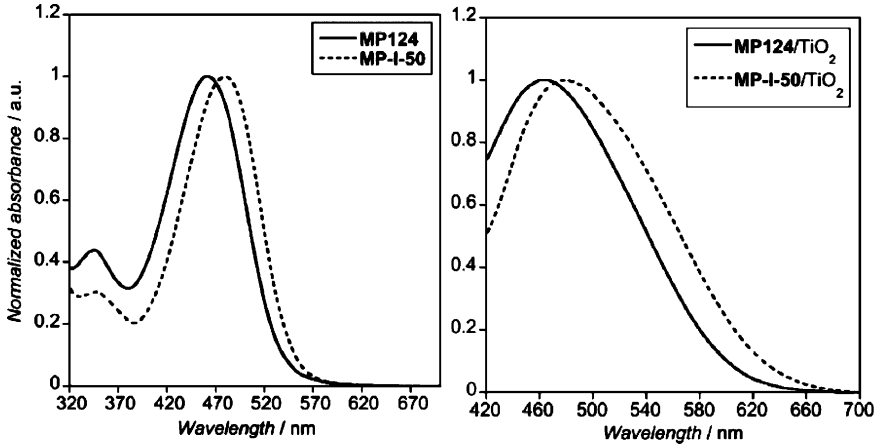

Figure 7. Normalized UV−visible spectra of MP124 (solid line) and MP-I-50 (dashed line) in ACN/*t*BuOH with 2% TEA (left) and on a nanocrystalline TiO_2 film (right). Reproduced from ref 62 with permission from the Royal Society of Chemistry.

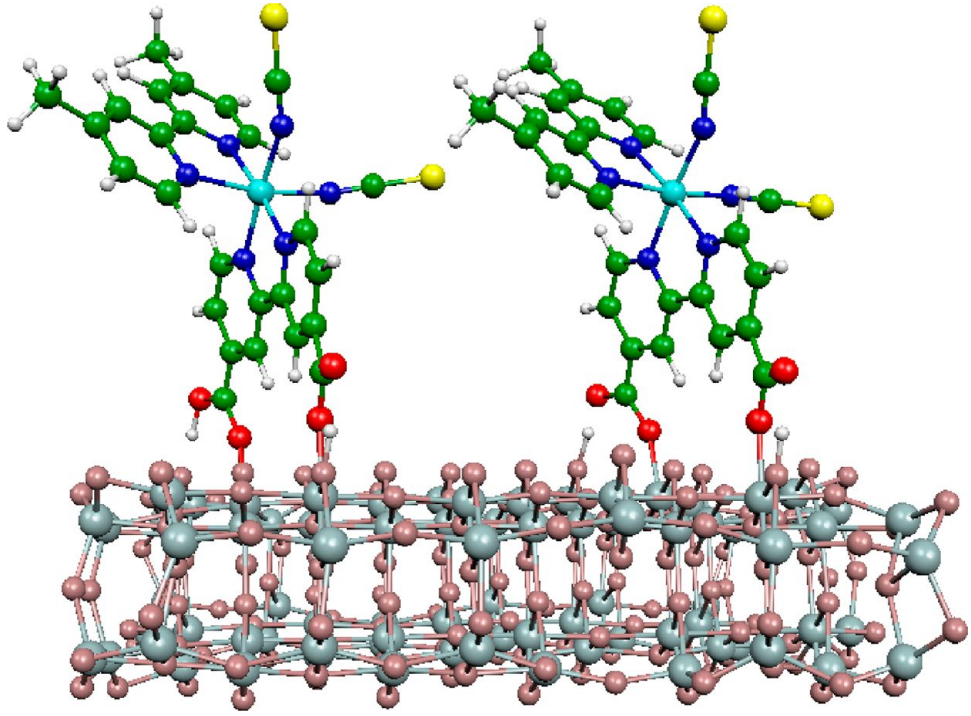

Figure 8. Optimized molecular structure of a dimeric configuration of the Z907 dye with nonyl chains replaced by methyl groups, adsorbed on the $(TiO_2)_{82}$ cluster.

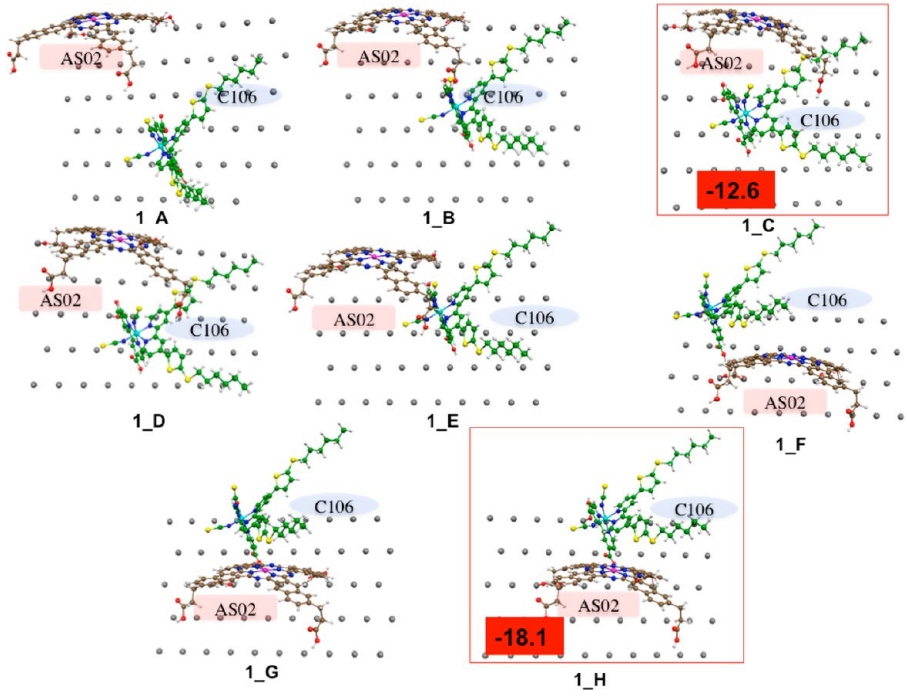

Figure 9. Top view of the 1:1 coadsorption schemes; the most stable structures are shown within red frames along with their interaction energies in kcal/mol in vacuo. In all cases, the AS02 and C106 dyes are bound to TiO_2 via two carboxylic groups. AS02 shows two bridged bidentate anchoring modes, while C106 shows two monodentate anchoring modes.

eV. Although this result might be sensitive to the choice of basis set (the 3-21G* basis is indeed close to a minimal choice), the calculated value is consistent with the very efficient hole transfer measured for this dye upon adsorption onto TiO_2[79] and, as suggested by the same authors, it is most likely the consequence of the proximity of the NCS ligands of the two interacting dyes.

Cosensitization of TiO_2. For the simulation of more complex aggregation patterns, composed of, for instance, three or more dye sensitizers, one needs to further extend the model and to increase the TiO_2 surface available for the dye adsorption. Obviously, the computational overhead associated with the growing size of the system becomes easily unaffordable. We recall indeed that a doubling of the system size implies with

dx.doi.org/10.1021/jz302147v | J. Phys. Chem. Lett. 2013, 4, 956−974

standard DFT implementations a ∼1 order of magnitude growth of the computational cost. The strategy we thus propose for the modeling of complex coadsorption schemes,[105] and that we shall widely discuss in the next section, consists of taking the structures of the sensitizers optimized alone on the $(TiO_2)_{82}$ cluster, removing the TiO_2 slab, and placing the calculated dye structures on a grid of Ti atoms with the same geometrical arrangement calculated for the $(TiO_2)_{82}$ cluster, in such a way to obtain a map of actual anchoring positions to place the dyes.[105] This model, based on a simple replication of the structure of the isolated anchored dye, clearly neglects the geometrical relaxation due to the intermolecular interactions as well as possible local relaxation of the TiO_2 surface due to the dye multiple anchoring. The basic idea consists of considering the dye adsorption mode as essentially determined by the specific dye−TiO_2 interactions, assumed to be identical for each surface Ti atom, and to calculate dye−dye intermolecular interactions a posteriori.

TiO_2 Cosensitized by Different Dyes. As mentioned in the introduction, the mixture of sensitizers having complementary absorption spectra, one of them possibly possessing high light-harvesting capability in the red and NIR regions, represents an appealing strategy to obtain panchromatic TiO_2 sensitization.[21−32] An alternative approach is that of exploiting FRET[104] from an energy relay dye (ERD) to the sensitizing dye (SD) to produce additional photocurrent.[103,163] FRET is mediated by the coupling of two resonant dipoles in the presence of an electric field,[103] and hence, the relative orientation of FRET donor and acceptor partners is crucial in determining the energy-transfer rate (see the Supporting Information for more details).

In a recent work, Hardin et al.[100] have reported on the energy transfer between a zinc naphthalocyanine ERD (AS02) and a Ru(II) SD (C106), both grafted onto the TiO_2 surface. Motivated by this study, we have modeled the cosensitization process by taking the optimized structures of the TiO_2-adsorbed standalone dyes and replicating these structures on the grid of Ti atoms presented above (additional technical details are given in section S1.5 in the Supporting Information).[105] Obviously, this approximation, necessary to model complex coadsorption schemes, neglects the structural relaxation of the dye ensembles due to the intermolecular interactions and is grounded on the assumption that in the sensitizing process, the dominant contribution is the dye−TiO_2 covalent interaction, which governs the dye anchoring mode and the orientation with respect to the surface. Although we have developed this strategy for the particular case illustrated here, the methodology is absolutely general, and as such, it can be extended to any cocktail of cosensitizing dyes, provided that one knows the relative surface coverage of each species.

Starting from 1:1 AS02/C106 arrangements and arriving to consider 1:4 AS02/C106 coadsorbed schemes, which mimic the reference experimental coverages of ∼80 (C106) and ∼20% (AS02), we selected the set of the most closely interacting configurations. To limit the variables in the coadsorption pattern selection, we followed a stepwise procedure; we started by selecting the two most stable "back" and "front" 1:1 dimeric structures to provide a suitable 1:2 trimeric aggregate (Figure 9). We then explored various possible positions for the third C106 molecule (Figure 10), selecting the most stable configuration. Finally, we looked for the most stable 1:4 AS02/C106 coadsorption aggregate (Figure 11), which reproduces the experimental relative coverage of the two

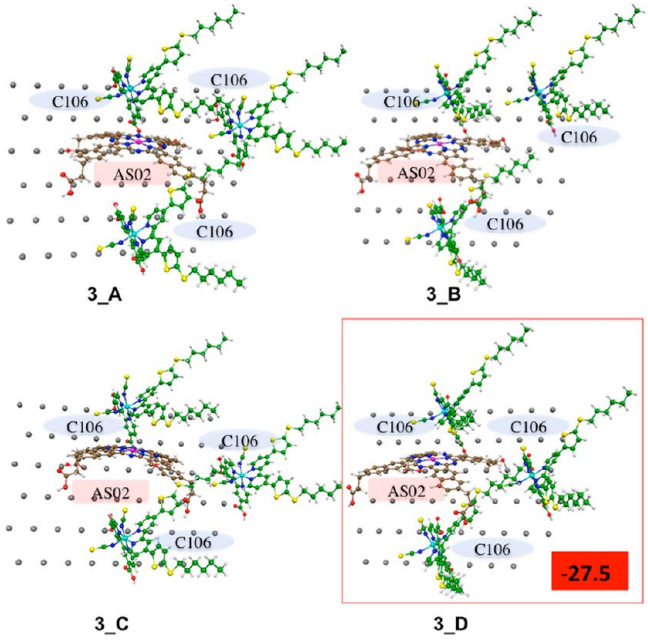

Figure 10. Top view of the 1:3 coadsorption schemes; the most stable structure is shown within a red frame along with its interaction energies in kcal/mol in vacuo. In all cases, the AS02 and C106 dyes are bound to TiO_2 via two carboxylic groups. AS02 shows two bridged bidentate anchoring modes, while C106 shows two monodentate anchoring modes.

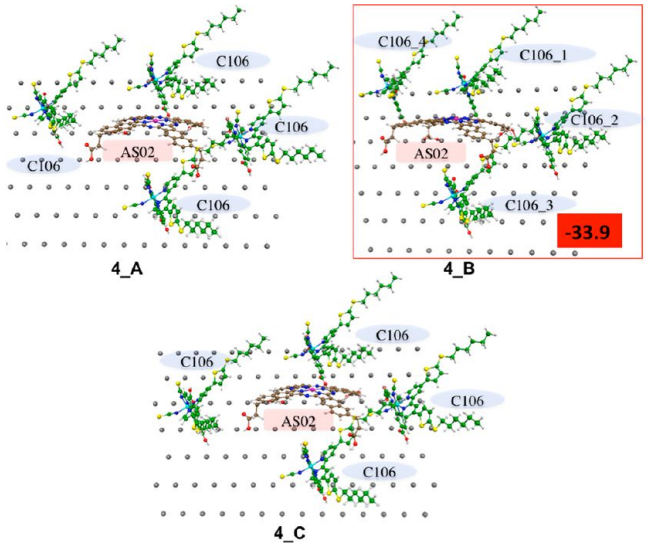

Figure 11. Top view of the 1:4 coadsorption schemes; the most stable structure is shown within a red frame along with its interaction energies in kcal/mol in vacuo. In all cases, the AS02 and C106 dyes are bound to TiO_2 via two carboxylic groups. AS02 shows two bridged bidentate anchoring modes, while C106 shows two monodentate anchoring modes.

species. We label the aggregate structures as *n*_X, with *n* ranging from 1 to 4, representing the number of SDs surrounding the ERD, and X (A−D) representing the different investigated interaction patterns. On the technical side, we note again the different interaction energies obtained by B3LYP and D3-B3LYP;[77] the inclusion of the D3 correction, accounting for dispersion interactions, provides a coherent trend within the calculated values, with an interaction energy increasing as the

dx.doi.org/10.1021/jz302147v | J. Phys. Chem. Lett. 2013, 4, 956−974

number of SD molecules increases, with the only exception of the 1:2 structure, given by combining the most stable 1_C and 1_H 1:1 (SD/ERD) assemblies, which turns out to be less stable than the constituents 1:1 structures due to a repulsive interaction between the two C106 molecules. Moving to the 1:3 cosensitization patterns (Figure 10), we find three assemblies (3_A, 3_C, and 3_D) to be very close in energy, with a stabilization energy of about 27 kcal/mol and relative differences within 0.8 kcal/mol. For the 1:4 aggregates (Figure 11), the 4_B structure is the most stable one, with a B3LYP-D3 stabilization energy of almost −34 kcal/mol. Our coadsorption scheme also predicts an average SD-ERD separation very close to the experimentally estimated value of ∼0.914 nm;[100] for the closest interacting AS02-C106 couple (1_H), we obtained a Zn−Ru distance of 0.908 nm, while for the 1_C configuration, the calculated Zn−Ru separation was 1.221 nm.

Table 4. Computed Interaction Energies (kcal/mol) of the Coadsorption Configurations of AS02 and C106[a]

	stabilization energy (kcal/mol)	
configurations	B3LYP	B3LYP+D3
1:1 AS02/C106 structures		
1_A	−2.4	−2.7
1_B	−7.7	−9.7
1_C	−6.8	**−12.6**
1_D	**−7.7**	−10.1
1_E	+5.7	−1.0
1_F	−2.9	−10.4
1_G	+14.0	−3.3
1_H	**−8.9**	**−18.1**
1:2 AS02/C106 structures		
2_A	**+4.6**	**−10.6**
1:3 AS02/C106 structures		
3_A	−9.1	−26.7
3_B	−3.0	−20.0
3_C	**−10.3**	−27.2
3_D	+0.3	**−27.5**
1:4 AS02/C106 structures		
4_A	−2.5	−32.3
4_B	**−3.4**	**−33.9**
4_C	+10.4	−18.3

[a]For each 1:*n* AS02/C106 ratio, the energy of the most stable configuration is highlighted in bold.

Finally, as discussed above for the indoline dyes, having determined the adsorption patterns on the oxide surface, we can try to reproduce the optical properties of the cosensitized assemblies. The experimental absorption spectra of the cosensitized TiO_2 (∼20% of AS02 and 80% of C106) showed a slight red shift and a small intensity decrease of the naphtalocyanine absorption peak as well as, although to a lesser extent, of the C106 absorption maximum.[100] The spectral shifts observed for the cosensitized system were attributed to the weak electronic interaction between the SD and ERD occurring for the TiO_2-anchored systems. Using the TiO_2-adsorbed geometries, for the isolated AS02 and C106 in solution, we calculated absorption maxima at 766 and 531 nm, respectively (see Figure 12, red and blue lines, respectively), which nicely reproduce the experimentally measured absorption peaks located at 773 (AS02) and 550 nm (C106).[100] As shown in the top panels of Figure 12, going from the simulated spectrum of the isolated AS02 ERD to those of the 1_H, 2_A, and 3_D cosensitized structures, our model progressively reproduces the red shift and the intensity decrease of the ERD main absorption band. For 3_D, we calculated an adsorption maximum of 770 nm, to be compared to the 766 nm value obtained for the isolated ERD. The agreement between the calculated and experimental spectral response associated with the formation of the coadsorbed AS02-C106 monolayer suggests that our model provides a realistic picture of the cosensitization pattern on TiO_2, properly describing the SD/ERD interactions. Most notably, by calculating the κ^2 orientational parameter (see eq 3 and Figure S2 in the Supporting Information) for the most interacting D−A couple (AS02-C106_1 in Figure 11) and using the calculated ERD/SD distance, we corrected the experimental Föster radius and predicted a FRET rate that is numerically the same as that obtained in ref 100, confirming the adequacy of the computational approach. We also showed that unfavorable ERD/SD orientations with very low κ^2 values and large distances, like, for instance, the AS02-C106_2 couple (Figure 11), yield sizable reductions in the FRET rates, up to 3 orders of magnitude.

Dye−Coadsorbent Cosensitized TiO_2. As a final application of our cosensitization modeling strategy described above, we report new results obtained for the simulations of the interaction between a surface-adsorbed organic dye and the most employed antiaggregation coadsorbent chenodeoxycholic acid (CDCA).[91,92] Experimentally, this is the most straightforward strategy to suppress dye aggregation on the TiO_2 surface, that is, to add to the dye solution a species that competes with the sensitizer in the adsorption process on the titania surface. We note that more recently, other coadsorbates, yielding to notably improved cell performances, have also been reported.[9,93,94]

Hara and co-workers reported the significant improvement of the photovoltaic performances of coumarine dyes (NKX series), prone to give aggregation upon adsorption onto TiO_2, when employing a high concentration of CDCA up to reach a decrease in the dye coverage by ∼50%.[97,164] Despite the high solubility of CDCA and the $\pi-\pi$ stacking interactions among the adsorbed NKX dyes, the progressive decrement of the dye loading when the CDCA concentration increases suggests that the intermolecular interactions between the CDCA and the NKX dye molecules, as well as the binding energies of CDCA to TiO_2, are somehow of comparable strength (or only slightly lower) to those between NKX molecules and NKX and TiO_2.

Using the coadsorption scheme presented above for the cosensitzed TiO_2, here, we calculate the interaction energies of NKX−NKX and CDCA−NKX dimers, considering among all of the possible configurations the closest interacting ones with no explicit atomic superimposition. As for the cases above, the dimers were built by taking the structures of the standalone optimized dyes on the $(TiO_2)_{82}$ slab and placing them on a grid of Ti atoms reproducing the active sites of the (101) anatase surface. The selected pattern, corresponding to the (−1,1) configuration according to the nomenclature illustrated in Figure S1 in the Supporting Information, is displayed in Figure 13, along with the relative B3LYP-D3 interaction energies and the optimized structure of the NKX@$(TiO_2)_{82}$ and CDCA@$(TiO_2)_{82}$ systems. Interestingly, the calculated interaction energy in the gas phase of the CDCA−NKX dimer (ca. 8 kcal/mol) is almost twice that of the NKX−NKX one (ca. 5 kcal/mol), suggesting a favorable coadsorption of CDCA and NKX molecules and an effective breaking of the NKX−NKX stacking

dx.doi.org/10.1021/jz302147v | J. Phys. Chem. Lett. 2013, 4, 956−974

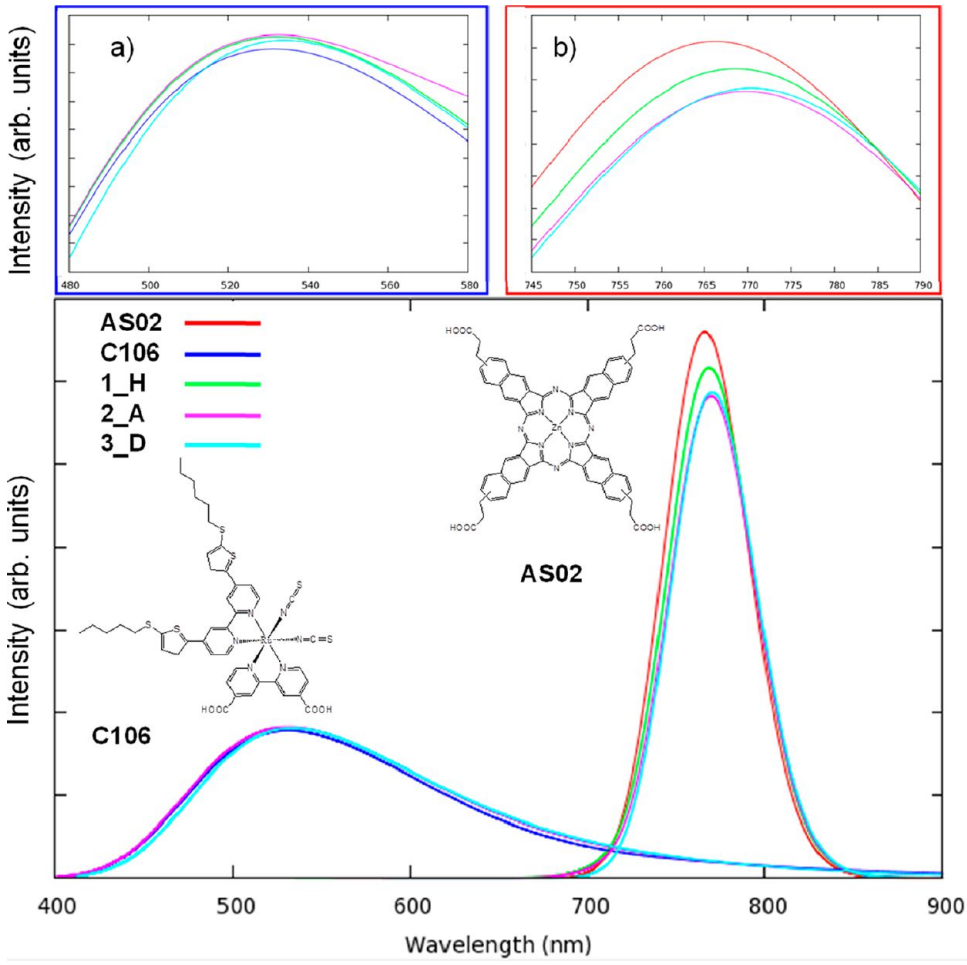

Figure 12. (Top) The two insets report the band maxima shifts for C106 (a) and AS02 (b). The spectra of C106 and AS02 have been simulated by a Gaussian broadening with σ = 0.05 and 0.20, respectively. In order to reproduce the experimental ratio between the C106 and AS02 extinction coefficients of about 1:5, the computed intensities of C106 were multiplied by a factor of 5. (Bottom) Calculated absorption spectra in water of isolated AS02 (red line) and C106 (blue line) sensitizers as well as those of the 1_H (light green line), 2_A (magenta line), and 3_D (cyano line) configurations.

by the coadsorbent. We notice, however, that such a strong interaction might be specific to the NKX sensitizer because it partly relies on the formation of a hydrogen bond, highlighted with a red circle in Figure 13, between the hydroxyl group of the CDCA and the carbonyl group of NKX, which are found at a distance of about 3 Å.

In conclusion, we have presented a unified overview of our recent activity on the computational modeling of relevant intermolecular interactions occurring in DSCs. The DSC is an inherent complex system, whose efficiency is essentially determined by the interrelated phenomena occurring at the multiple molecular−semiconductor−electrolyte heterointerfaces. As such, while DSCs can be idealized as being formed by three fundamental components (i.e., the dye, the metal oxide, and the redox shuttle), which, to a first approximation, can be individually optimized in the continuing search for higher photovoltaic efficiency or longer device temporal stability, in most real cases, the interdependencies and interactions among the various components dictate the overall device performances.

While DSCs can be idealized as being formed by three fundamental components (i.e., the dye, the metal oxide, and the redox shuttle), which, to a first approximation, can be individually optimized in the continuing search for higher photovoltaic efficiency or longer device temporal stability, in most real cases, the interdependencies and interactions among the various components dictate the overall device performances.

Relevant pair interactions include, but are possibly not limited to, (i) Dye−semiconductor, (ii) redox shuttle−semiconductor, (iii) dye−redox shuttle, and (iv) dye−dye and dye−coadorbents interactions. The interaction between the sensitizing dye and the semiconductor is related to the primary charge generation event in DSCs, that is, the dissociation of the dye molecular exciton following electron injection from the dye excited state into the manifold of semiconductor unoccupied

dx.doi.org/10.1021/jz302147v | J. Phys. Chem. Lett. 2013, 4, 956−974

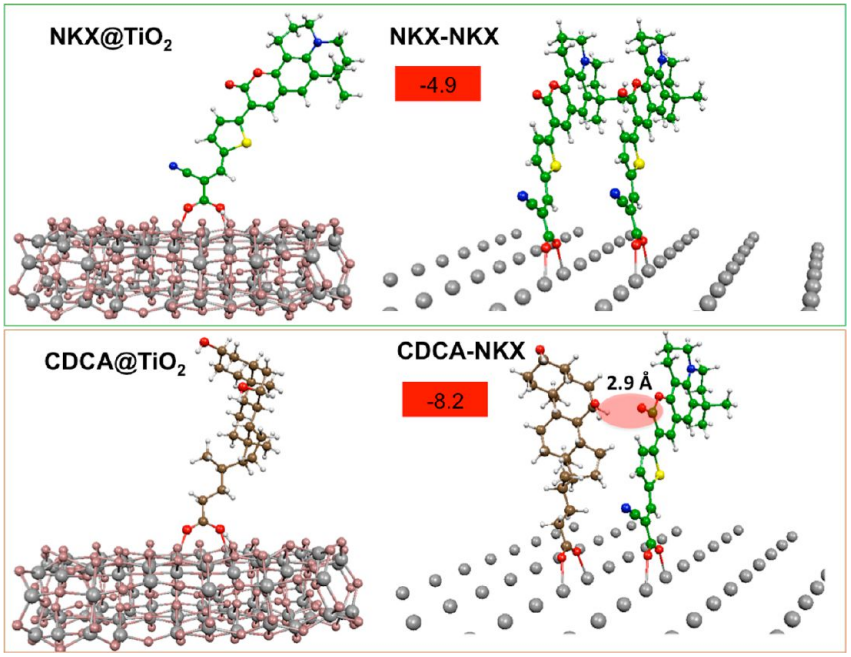

Figure 13. (Left) Optimized ground-state geometries of NKX@$(TiO_2)_{82}$ (up panel) and CDCA@$(TiO_2)_{82}$ (bottom panel) in the bidentate bridged mode. (Right) A close interacting dimeric configurations of NKX−NKX (upper panel) and CDCA−NKX (lower panel) and their interaction energies (kcal/mol).

states. The main redox shuttle−semiconductor interactions relevant in DSCs are those occurring between potential-determining ions in the electrolyte solution (e.g., Li^+).[53,54] Also, the nature of the electrolyte solvent might directly or indirectly (e.g., by the solvent acid/base chemistry) affect the semiconductor. Dye−redox shuttle interactions have been invoked in many instances to explain the correlation between structural/chemical dye variations and their functioning in DSC devices. In particular, some authors[60−65] suggested the idea that particular atoms or chemical groups can also provide binding sites for I_2 (I_3^-), increasing its concentration close to the TiO_2 surface and thus accelerating the recombination and/or dye regeneration processes.

Dye−dye intermolecular interactions are of paramount importance in determining the overall DSC conversion efficiency because they significantly affect the charge generation and may inhibit recombination reactions, whereby a compact dye monolayer would act as an insulating layer toward the approach of the redox shuttle electrolyte to the semiconductor surface. Strong dye−dye intermolecular interactions, however, introduce undesired effects, such as a filtering effect by non-surface-adsorbed dye molecules and intermolecular excited-state quenching. Even more important, dye−dye intermolecular interactions are fundamental in determining the fate of cosensitized DSCs, in which two different dyes have to be accommodated on the TiO_2 surface in an optimal ratio.

Conventional spectroelectrochemical and photovoltaic measurements offer an a posteriori verification of the interdependencies among the various DSC components (e.g., a broader UV−vis absorption spectrum for a dye-sensitized electrode usually signals a dense dye packing aggregation), while a specific characterization of the intermolecular interactions taking place at the relevant heterointerfaces requires more sophisticated investigations (e.g., PES, SERS, FT-IR), which are not conventionally applicable to real DSC devices.

Computational modeling can offer an alternative view of the interface and deliver hitherto inaccessible detailed information on the atomistic scale, assisting the design of new sensitizers and providing a deeper comprehension of the basic chemical physics processes governing the cell functioning and its performances. A computational approach to DSC modeling can be essentially casted into a stepwise problem, whereby one first needs to accurately simulate the individual DSC components to move to the relevant pair (or higher-order) interactions discussed above.

In this Perspective, we have illustrated the basic methodology and selected applications of computational modeling of dye−dye and dye−coadsorbent intermolecular interactions taking place at the dye-sensitized interface. The results from previous investigations have been reviewed, integrating previous calculations with new ones to offer a critical assessment of the computational results. We have shown that the proposed methodology offers a realistic picture of aggregation phenomena among surface-adsorbed dyes, as revealed by the accurate reproduction of the optical response of aggregates of different dyes, characterized by different anchoring groups. The reliability of the aggregation pattern for indoline dyes is also corroborated by the reproduction of the experimentally observed Stark shifts, which we attribute to the presence of closely interacting neutral and oxidized surface-adsorbed dyes.

A strategy to approach the structural and electronic properties of cosensitized semiconductor interfaces has then been presented, illustrating the impact of intermolecular interactions between different surface-adsorbed species on FRET from an ERD to a SD and the antiaggregation effect of chenodeoxycholic acid (CDCA). The accuracy of the cosensitization pattern on TiO_2 is corroborated by the agreement between the calculated and experimental optical spectral responses associated with the formation of coadsorbed FRET partners and by the reproduction of the experimental

dx.doi.org/10.1021/jz302147v | J. Phys. Chem. Lett. 2013, 4, 956−974

FRET rate based on calculated geometrical arrangement and structural parameters.

The information acquired from these studies might constitute the basis for an integrated multiscale computational description of the device functioning, including all of the possible interdependencies among the DSC constituents, which may further boost the DSC efficiency along with providing the basic understanding of the device necessary to further enhance priority DSC requirements, such as temporal stability and optimization of device components. We believe that this direction should be the target of future computational modeling research in the DSCs field.

■ ASSOCIATED CONTENT

Supporting Information

Model and computational details. This material is available free of charge via the Internet at http://pubs.acs.org.

■ AUTHOR INFORMATION

Corresponding Author

*E-mail: chiara@thch.unipg.it (M.P.): filippo@thch.unipg.it (F.D.A.).

Notes

The authors declare no competing financial interest.

Biographies

Mariachiara Pastore obtained her Ph.D. in 2009 in theoretical chemistry from the University of Ferrara, working in the multireference perturbation methods field. Currently, she is an associate postdoc at the CNR-ISTM of Perugia. Her main research interests concern the computational modeling of the spectroscopic properties of dyes and dye−TiO_2 interfaces. Web-page: http://www.clhyo.org/people/5-mariachiara-pastore.html

Filippo De Angelis is senior research scientist and deputy director at the CNR Institute of Molecular Sciences and Technology in Perugia, Italy. He is the founder of the Computational Laboratory for Hybrid/Organic Photovoltaics. He is an expert in the simulation of materials and processes in dye-sensitized solar cells. Web page: http://www.clhyo.org/

■ ACKNOWLEDGMENTS

We thank FP7-NMP-2009 project 246124 "SANS" and FP7-ENERGY-2010 project 261920 "ESCORT" for financial support. We thank MIUR-PRIN 2008, project 2008CSNZFR for a grant. We also thank Edoardo Mosconi for helpful discussions.

■ REFERENCES

(1) O'Regan, B.; Grätzel, M. A Low-Cost, High-Efficiency Solar Cell Based on Dye-Sensitized Colloidal TiO_2Films. *Nature* **1991**, *353*, 737−740.

(2) Grätzel, M. Recent Advances in Sensitized Mesoscopic Solar Cells. *Acc. Chem. Res.* **2009**, *42*, 1788−1798.

(3) Hagfeldt, A.; Boschloo, G.; Sun, L.; Kloo, L.; Pettersson, H. Dye-Sensitized Solar Cells. *Chem. Rev.* **2010**, *110*, 6595−6663.

(4) Hardin, B. E.; Snaith, H. J.; McGehee, M. D. The Renaissance of Dye-Sensitized Solar Cells. *Nat. Photonics* **2012**, *6*, 162.

(5) Nazeeruddin, M. K.; Kay, A.; Rodicio, I.; Humphry-Baker, R.; Mueller, E.; Liska, P.; Vlachopoulos, N.; Graetzel, M. Conversion of Light to Electricity by *cis*-X_2Bis(2,2′-bipyridyl-4,4′-dicarboxylate)-ruthenium(II) Charge-Transfer Sensitizers (X = Cl^-, Br^-, I^-, CN^-, and SCN^-) on Nanocrystalline Titanium Dioxide Electrodes. *J. Am. Chem. Soc.* **1993**, *115*, 6382−6390.

(6) Nazeeruddin, M. K.; De Angelis, F.; Fantacci, S.; Selloni, A.; Viscardi, G.; Liska, P.; Ito, S.; Takeru, B.; Grätzel, M. Combined Experimental and DFT-TDDFT Computational Study of Photoelectrochemical Cell Ruthenium Sensitizers. *J. Am. Chem. Soc.* **2005**, *127*, 16835−16847.

(7) Nazeeruddin, M. K.; Péchy, P.; Grätzel, M. Efficient Panchromatic Sensitization of Nanocrystalline TiO_2 Films by a Black Dye Based on Atrithiocyanato−Ruthenium Complex. *Chem Commun* **1997**, 1705−1706.

(8) Nazeeruddin, M. K.; Péchy, P.; Renouard, T.; Zakeeruddin, S. M.; Humphry-Baker, R.; Comte, P.; Liska, P.; Cevey, L.; Costa, E.; Shklover, V.; et al. Engineering of Efficient Panchromatic Sensitizers for Nanocrystalline TiO_2-Based Solar Cells. *J. Am. Chem. Soc.* **2001**, *123*, 1613−1624.

(9) Han, L.; Islam, A.; Chen, H.; Malapaka, C.; Chiranjeevi, B.; Zhang, S.; Yang, X.; Yanagida, M. High-Efficiency Dye-Sensitized Solar Cell with a Novel Co-Adsorbent. *Energy Environ. Sci.* **2012**, *5*, 6057−6060.

(10) Wang, P.; Zakeeruddin, S. M.; Exnar, I.; Grätzel, M. High Efficiency Dye-Sensitized Nanocrystalline Solar Cells Based on Ionic Liquid Polymer Gel Electrolyte. *Chem Commun* **2002**, 2972−2973.

(11) Chen, C.-Y.; Wu, S.-J.; Wu, C.-G.; Chen, J.-G.; Ho, K.-C. A Ruthenium Complex with Superhigh Light-Harvesting Capacity for Dye-Sensitized Solar Cells. *Angew. Chem., Int. Ed.* **2006**, *45*, 5822−5825.

(12) Gao, F.; Wang, Y.; Shi, D.; Zhang, J.; Wang, M.; Jing, X.; Humphry-Baker, R.; Wang, P.; Zakeeruddin, S. M.; Grätzel, M. Enhance the Optical Absorptivity of Nanocrystalline TiO_2 Film with High Molar Extinction Coefficient Ruthenium Sensitizers for High Performance Dye-Sensitized Solar Cells. *J. Am. Chem. Soc.* **2008**, *130*, 10720−10728.

(13) Bessho, T.; Yoneda, E.; Yum, J.-H.; Guglielmi, M.; Tavernelli, I.; Imai, H.; Rothlisberger, U.; Nazeeruddin, M. K.; Grätzel, M. New Paradigm in Molecular Engineering of Sensitizers for Solar Cell Applications. *J. Am. Chem. Soc.* **2009**, *131*, 5930−5934.

(14) Bomben, P. G.; Koivisto, B. D.; Berlinguette, C. P. Cyclometalated Ru Complexes of Type $[Ru^{II}(N\text{^}N)_2(C\text{^}N)]^z$: Physicochemical Response to Substituents Installed on the Anionic Ligand. *Inorg. Chem.* **2010**, *49*, 4960−4971.

(15) Mishra, A.; Fischer, M.; Bäuerle, P. Metal-Free Organic Dyes for Dye-Sensitized Solar Cells: From Structure: Property Relationships to Design Rules. *Angew. Chem., Int. Ed.* **2009**, *48*, 2474−2499.

(16) Pastore, M.; Mosconi, E.; Fantacci, S.; De Angelis, F. Computational Investigations on Organic Sensitizers for Dye-Sensitized Solar Cells. *Curr. Org. Synth.* **2012**, *9*, 215−232.

(17) Zeng, W.; Cao, Y.; Bai, Y.; Wang, Y.; Shi, Y.; Zhang, M.; Wang, F.; Pan, C.; Wang, P. Efficient Dye-Sensitized Solar Cells with an Organic Photosensitizer Featuring Orderly Conjugated Ethylenedioxythiophene and Dithienosilole Blocks. *Chem. Mater.* **2010**, *22*, 1915−1925.

(18) Wu, S.-L.; Lu, H.-P.; Yu, H.-T.; Chuang, S.-H.; Chiu, C.-L.; Lee, C.-W.; Diau, E. W.-G.; Yeh, C.-Y. Design and Characterization of Porphyrin Sensitizers with a Push−Pull Framework For Highly Efficient Dye-Sensitized Solar Cells. *Energy Environ. Sci.* **2010**, *3*, 949−955.

(19) Chang, Y.-C.; Wang, C.-L.; Pan, T.-Y.; Hong, S.-H.; Lan, C.-M.; Kuo, H.-H.; Lo, C.-F.; Hsu, H.-Y.; Lin, C.-Y.; Diau, E. W.-G. A Strategy to Design Highly Efficient Porphyrin Sensitizers for Dye-Sensitized Solar Cells. *Chem. Commun.* **2011**, *47*, 8910−8912.

(20) Yella, A.; Lee, H.-W.; Tsao, H. N.; Yi, C.; Chandiran, A. K.; Nazeeruddin, M. K.; Diau, E. W.-G.; Yeh, C.-Y.; Grätzel, M. Porphyrin-Sensitized Solar Cells with Cobalt (II/III)-Based Redox Electrolyte Exceed 12% Efficiency. *Science* **2011**, *4*, 629−634.

(21) Clifford, J. N.; Forneli, A.; Chen, H.; Torres, T.; Tan, S.; Palomares, E. Co-Sensitized DSCs: Dye Selection Criteria for Optimized Device V_{oc} and Efficiency. *J. Mater. Chem.* **2011**, *21*, 1693−1696.

(22) Sayama, K.; Tsukagoshi, S.; Mori, T.; Hara, K.; Ohga, Y.; Shinpou, A.; Abe, Y.; Suga, S.; Arakawa, H. Efficient Sensitization of

Nanocrystalline TiO_2 Films with Cyanine and Merocyanine Organic Dyes. *Sol. Energy Mater. Sol. Cells* **2003**, *80*, 47−71.
(23) Martínez-Díaz, M. V.; de la Torre; Torres, T. Lighting Porphyrins and Phthalocyanines for Molecular Photovoltaics. *Chem Commun.* **2010**, *46*, 7090−7108.
(24) Chen, Y.; Zeng, Z.; Li, C.; Wang, W.; Wang, X.; Zhang, B. Highly Efficient Co-Sensitization of Nanocrystalline TiO_2 Electrodes with Plural Organic Dyes. *New. J. Chem.* **2005**, *29*, 773−776.
(25) Yum, J.-H.; Jang, S.-R.; Walter, P.; Geiger, T.; Nüesch, F.; Kim, S.; Ko, J.; Grätzel, M.; Nazeeruddin, M. K. Efficient Co-Sensitization of Nanocrystalline TiO_2 Films by Organic Sensitizers. *Chem. Commun.* **2007**, 4680−4682.
(26) Lan, C.-M.; Wu, H.-P.; Pan, T.-Y.; Chang, C.-W.; Chao, W.-S.; Chen, C.-T.; Wang, C.-L.; Lin, C.-Y.; Diau, E. W.-G. Enhanced Photovoltaic Performance with Co-Sensitization of Porphyrin and an Organic Dye in Dye-Sensitized Solar Cells. *Energy Environ. Sci.* **2012**, *5*, 6460−6464.
(27) Yum, J.-H.; Baranoff, E.; Wenger, S.; Nazeeruddin, M. K.; Grätzel, M. Panchromatic Engineering for Dye-Sensitized Solar Cells. *Energy Environ. Sci.* **2011**, *4*, 842−857.
(28) Brown, M. D.; Parkinson, P.; Torres, T.; Miura, H.; Herz, L. M.; Snaith, H. J. Surface Energy Relay Between Cosensitized Molecules in Solid-State Dye-Sensitized Solar Cells. *J. Phys. Chem. C* **2011**, *115*, 23204−23208.
(29) Siegers, C.; Würfel, U.; Zistler, M.; Gores, H.; Hohl-Ebinger, J.; Hinsch, A.; Haag, R. Overcoming Kinetic Limitations of Electron Injection in the Dye Solar Cell via Coadsorption and FRET. *Chem. Phys. Chem.* **2008**, *9*, 793−798.
(30) Clifford, J. N.; Palomares, E.; Nazeeruddin, M. K.; Thampi, R.; Grätzel, M.; Durrant, J. R. Multistep Electron Transfer Processes on Dye Co-sensitized Nanocrystalline TiO_2 Films. *J. Am. Chem. Soc.* **2004**, *126*, 5670−5671.
(31) Fan, S.-Q.; Kim, C.; Fang, B.; Liao, K.-X.; Yang, G.-J.; Li, C.-J.; Kim, J.-J.; Ko, J. Improved Efficiency of over 10% in Dye-Sensitized Solar Cells with a Ruthenium Complex and an Organic Dye Heterogeneously Positioning on a Single TiO_2 Electrode. *J. Phys. Chem. C* **2011**, *115*, 7747−7754.
(32) Ogura, R. Y.; Nakane, S.; Morooka, M.; Orihashi, M.; Suzuki, Y.; Noda, K. High-Performance Dye-Sensitized Solar Cell with a Multiple Dye System. *Appl. Phys. Lett.* **2009**, *94*, 073308.
(33) Ozawa, H.; Shimizu, R.; Arakawa, H. Significant Improvement in the Conversion Efficiency of Black-Dye-Based Dye-Sensitized Solar Cells by Cosensitization with Organic Dye. *RSC Adv.* **2012**, *2*, 3198−3200.
(34) Kuang, D.; Walter, P.; Nüesch, F.; Kim, S.; Ko, J.; Comte, P.; Zakeeruddin, S. M.; Nazeeruddin, M. K.; Grätzel, M. Co-sensitization of Organic Dyes for Efficient Ionic Liquid Electrolyte-Based Dye-Sensitized Solar Cells. *Langmuir* **2007**, *23*, 10906−10909.
(35) Nguyen, L. H.; Mulmudi, H. K.; Sabba, D.; Kulkarni, S. A.; Batabyal, S. K.; Nonomura, K.; Grätzel, M.; Mhaisalkar, S. G. A Selective Co-Sensitization Approach to Increase Photon Conversion Efficiency and Electron Lifetime in Dye-Sensitized Solar Cells. *Phys. Chem. Chem. Phys.* **2012**, *14*, 16182−16186.
(36) Ito, S.; Chen, P.; Comte, P.; Nazeeruddin, M. K.; Liska, P.; Pechy, P.; Grätzel, M. Fabrication of Screen-Printing Pastes from TiO_2 Powders for Dye-Sensitised Solar Cells. *Progr. Photovoltaics* **2007**, *15*, 603−612.
(37) Shankar, K.; K Mor, G.; Prakasam, H. E.; Yoriya, S.; Paulose, M.; Varghese, O. K.; Grimes, C. A. Highly-Ordered TiO_2 Nanotube Arrays up to 220 μm in Length: Use in Water Photoelectrolysis and Dye-Sensitized Solar Cells. *Nanothecnology* **2007**, *18*, 065707.
(38) Saito, M.; Fujihara, S. Large Photocurrent Generation in Dye-Sensitized ZnO Solar Cells. *Energy Environ. Sci.* **2008**, *1*, 280−283.
(39) Keis, K.; Lindgren, J.; Lindquist, S.-E.; Hagfeldt, A. Studies of the Adsorption Process of Ru Complexes in Nanoporous ZnO Electrodes. *Langmuir* **2000**, *16*, 4688−4694.
(40) Ferrere, S.; Zaban, A.; Gregg, B. A. Dye Sensitization of Nanocrystalline Tin Oxide by Perylene Derivatives. *J. Phys. Chem. B* **1997**, *101*, 4490−4493.
(41) Kay, A.; Grätzel, M. Dye-Sensitized Core−Shell Nanocrystals: Improved Efficiency of Mesoporous Tin Oxide Electrodes Coated with a Thin Layer of an Insulating Oxide. *Chem. Mater.* **2002**, *14*, 2930−2935.
(42) O'Regan, B. C.; Durrant, J. R. Kinetic and Energetic Paradigms for Dye-Sensitized Solar Cells: Moving from the Ideal to the Real. *Acc. Chem. Res.* **2009**, *42*, 1799−1808.
(43) Persson, P.; Lundqvist, M. J.; Ernstorfer, R.; Goddard, W. A., III; Willig, F. Quantum Chemical Calculations of the Influence of Anchor-Cum-Spacer Groups on Femtosecond Electron Transfer Times in Dye-Sensitized Semiconductor Nanocrystals. *J. Chem. Theor. Comput.* **2006**, *2*, 441−451.
(44) Lundqvist, M. J.; Nilsing, M.; Lunell, S.; Åkermark, B.; Persson, P. Spacer and Anchor Effects on the Electronic Coupling in Ruthenium-bis-Terpyridine Dye-Sensitized TiO_2 Nanocrystals Studied by DFT. *J. Phys. Chem. B* **2006**, *110*, 20513−20525.
(45) Ambrosio, F.; Martsinovich, N.; Troisi, A. What Is the Best Anchoring Group for a Dye in a Dye-Sensitized Solar Cell? *J. Phys. Chem. Lett.* **2012**, *3*, 1531−1535.
(46) Grätzel, M. Conversion of Sunlight to Electric Power by Nanocrystalline Dye-Sensitized Solar Cells. *J. Photochem. Photobiol., A* **2004**, *164*, 3−14.
(47) Odobel, F.; Blart, E.; Lagrée, M.; Villieras, M.; Boujtita, H.; El Murr, N.; Caramori, S.; Bignozzi, C. A. Porphyrin Dyes for TiO_2 Sensitization. *J. Mater. Chem.* **2003**, *13*, 502−510.
(48) Abbotto, A.; Manfredi, N.; Marinzi, C.; De Angelis, F.; Mosconi, E.; Yum, J.; Xianxi, Z.; Nazeeruddin, M. K.; Grätzel, M. Di-Branched Di-Anchoring Organic Dyes for Dye-Sensitized Solar Cells. *Energy Environ. Sci.* **2009**, *2*, 1094.
(49) Ronca, E.; Pastore, M.; Belpassi, L.; Tarantelli, F.; De Angelis, F. Influence of the Dye Molecular Structure on the TiO_2 Conduction Band in Dye-Sensitized Solar Cells: Disentangling Charge Transfer and Electrostatic Effects. *Energy Environ. Sci.* **2013**, *6*, 183−193.
(50) Muscat, J. P.; Newns, D. M. Chemisorption on Metals. *Prog. Surf. Sci.* **1978**, *9*, 1−43.
(51) Lundqvist, M. J.; Nilsing, M.; Persson, P.; Lunel, S. DFT Study of Bare and Dye-Sensitized TiO_2 Clusters and Nanocrystals. *Int. J. Quantum Chem.* **2006**, *106*, 3214−3234.
(52) Ambrosio, F.; Martsinovich, N.; Troisi, A. Effect of the Anchoring Group on Electron Injection: Theoretical Study of Phosphonated Dyes for Dye-Sensitized Solar Cells. *J. Phys. Chem. C* **2012**, *116*, 2622−2629.
(53) Redmond, G.; Fitzmaurice, D. Spectroscopic Determination of Flatband Potentials for Polycrystalline Titania Electrodes in Non-aqueous Solvents. *J. Phys. Chem.* **1993**, *97*, 1426−1430.
(54) Boschloo, G.; Fitzmaurice, D. Electron Accumulation in Nanostructured TiO_2 (Anatase) Electrodes. *J. Phys. Chem. B* **1999**, *103*, 7860−7868.
(55) Kelly, C. A.; Farzad, F.; Thompson, D. W.; Stipkala, J. M.; Meyer, G. J. Cation-Controlled Interfacial Charge Injection in Sensitized Nanocrystalline TiO_2. *Langmuir* **1999**, *15*, 7047−7054.
(56) Pelet, S.; Moser, J.-E.; Grätzel, M. Cooperative Effect of Adsorbed Cations and Iodide on the Interception of Back Electron Transfer in the Dye Sensitization of Nanocrystalline TiO_2. *J. Phys. Chem. B* **2000**, *104*, 1791−1795.
(57) Koops, S. E.; O'Regan, B. C.; Barnes, P. R. F.; Durrant, J. R. Parameters Influencing the Efficiency of Electron Injection in Dye-Sensitized Solar Cells. *J. Am. Chem. Soc.* **2009**, *131*, 4808−4818.
(58) Rothenberger, G.; Fitzmaurice, D.; Grätzel, M. Spectroscopy of Conduction Band Electrons in Transparent Metal Oxide Semiconductor Films: Optical Determination of the Flatband Potential of Colloidal Titanium Dioxide Films. *J. Phys. Chem.* **1992**, *96*, 5983−5986.
(59) O'Regan, B.; Grätzel, M.; Fitzmaurice, D. Optical Electrochemistry. 2. Real-Time Spectroscopy of Conduction Band Electrons in a Metal Oxide Semiconductor Electrode. *J. Phys. Chem.* **1991**, *95*, 10525−10528.
(60) O'Regan, B. C.; Walley, K.; Juozapavicius, M.; Anderson, A. Y.; Matar, F.; Ghaddar, T.; Zakeeruddin, S. M.; Klein, C.; Durrant, J. R.

Structure/Function Relationships in Dyes for Solar Energy Conversion: A Two-Atom Change in Dye Structure and the Mechanism for Its Effect on Cell Voltage. *J. Am. Chem. Soc.* **2009**, *131*, 3541−3548.
(61) Miyashita, M.; Sunahara, K.; Nishikawa, K.; Uemura, Y.; Koumura, N.; Hara, K.; Mori, A.; Abe, T.; Suzuki, E.; Mori, S. Interfacial Electron-Transfer Kinetics in Metal-Free Organic Dye-Sensitized Solar Cells: Combined Effects of Molecular Structure of Dyes and Electrolytes. *J. Am. Chem. Soc.* **2008**, *130*, 17874−17881.
(62) Planells, M.; Pellejà, L.; Clifford, J. N.; Pastore, M.; De Angelis, F.; López, N.; Marder, S. R.; Palomares, E. Energy Levels, Charge Injection, Charge Recombination and Dye Regeneration Dynamics for Donor−Acceptor π-Conjugated Organic Dyes in Mesoscopic TiO_2 Sensitized Solar Cells. *Energy Environ. Sci.* **2011**, *4*, 1820−1829.
(63) Pastore, M.; Mosconi, E.; De Angelis, F. Computational Investigation of Dye−Iodine Interactions in Organic Dye-Sensitized Solar Cells. *J. Phys. Chem. C* **2012**, *116*, 5965−5973.
(64) Bai, Y.; Zhang, J.; Zhou, D.; Wang, Y.; Zhang, M.; Wang, P. Engineering Organic Sensitizers for Iodine-Free Dye-Sensitized Solar Cells: Red-Shifted Current Response Concomitant with Attenuated Charge Recombination. *J. Am. Chem. Soc.* **2011**, *133*, 11442−11445.
(65) Tuikka, M.; Hirva, P.; Rissanen, K.; Korppi-Tommola, J.; Haukka, M. Halogen Bonding—A Key Step in Charge Recombination of the Dye-Sensitized Solar Cell. *Chem. Commun.* **2011**, *47*, 4499−4501.
(66) Li, X.; Reynal, A.; Barnes, P.; Humphry-Baker, R.; Zakeeruddin, S. M.; De Angelis, F.; O'Regan, B. C. Measured Binding Coefficients for Iodine and Ruthenium Dyes; Implications for Recombination in Dye Sensitised Solar Cells. *Phy. Chem. Chem. Phys.* **2012**, *14*, 15421−15428.
(67) Mosconi, E.; Yum, J.-H.; Kessler, F.; García, C. J. G.; Zuccaccia, C.; Cinti, A.; Nazeeruddin, M. K.; Grätzel, M.; De Angelis, F. Cobalt Electrolyte/Dye Interactions in Dye-Sensitized Solar Cells: A Combined Computational and Experimental Study. *J. Am. Chem. Soc.* **2012**, *134*, 19438−19453.
(68) Xu, M.; Zhang, M.; Pastore, M.; Li, R.; De Angelis, F.; Wang, P. Joint Electrical, Photophysical and Computational Studies on D−π−A Dye Sensitized Solar Cells: The Impacts of Dithiophene Rigidification. *Chem. Sci.* **2012**, *3*, 976−983.
(69) Dualeh, A.; De Angelis, F.; Fantacci, S.; Moehl, T.; Yi, C.; Kessler, F.; Baranoff, E.; Nazeeruddin, M. K.; Grätzel, M. Influence of Donor Groups of Organic D−π−A Dyes on Open-Circuit Voltage in Solid-State Dye-Sensitized Solar Cells. *J . Phys. Chem. C* **2012**, *116*, 1572−1578.
(70) Howie, W. H.; Claeyssens, F.; Miura, H.; Peter, L. M. Characterization of Solid-State Dye-Sensitized Solar Cells Utilizing High Absorption Coefficient Metal-Free Organic Dyes. *J. Am. Chem. Soc.* **2008**, *130*, 1367−1375.
(71) De Angelis, F.; Vitillaro, G.; Kavan, L.; Nazeeruddin, M. K.; Grätzel, M. Modeling Ruthenium-Dye-Sensitized TiO_2 Surfaces Exposing the (001) or (101) Faces: A First-Principles Investigation. *J. Phys Chem. C* **2012**, *116*, 18124−18131.
(72) Griffith, M. J.; James, M.; Triani, G.; Wagner, P.; Wallace, G. G.; Officer, D. L. Determining the Orientation and Molecular Packing of Organic Dyes on a TiO_2 Surface Using X-ray Reflectometry. *Langmuir* **2011**, *27*, 12944−12950.
(73) Ellis-Gibbings, L.; Johansson, V.; Walsh, R. B.; Kloo, L.; Quinton, J. S.; Andersson, G. G. Formation of N719 Dye Multilayers on Dye Sensitized Solar Cell Photoelectrode Surfaces Investigated by Direct Determination of Element Concentration Depth Profiles. *Langmuir* **2012**, *28*, 9431−9439.
(74) Hahlin, M.; Johansson, E.; Plogmaker, S.; Odelius, M.; Sun, L.; Siegbahn, H.; Rensmo, H. Electronic and Molecular Structures of Organic Dye/TiO_2 Interfaces for Solar Cell Applications: A Core Level Photoelectron Spectroscopy Study. *Phys. Chem. Chem. Phys.* **2010**, *12*, 1507−1517.
(75) Pastore, M.; De Angelis, F. Computational Modelling of TiO_2 Surfaces Sensitized by Organic Dyes With Different Anchoring Groups: Adsorption modes, Electronic Structure and Implication for Electron Injection/Recombination. *Phy. Chem. Chem. Phys.* **2012**, *14*, 920−928.
(76) Anselmi, C.; Mosconi, E.; Pastore, M.; Ronca, E.; De Angelis, F. Adsorption of Organic Dyes on TiO_2 Surfaces in Dye-Sensitized Solar Cells: Interplay of Theory and Experiment. *Phy. Chem. Chem. Phys.* **2012**, *14*, 15963−15974.
(77) Pastore, M.; De Angelis, F. Aggregation of Organic Dyes on TiO_2 in Dye-Sensitized Solar Cells Models: An ab Initio Investigation. *ACS Nano* **2010**, *4*, 556−562.
(78) Fattori, A.; M. Peter, L.; Wang, H.; Miura, H.; Marken, F. Fast Hole Surface Conduction Observed for Indoline Sensitizer Dyes Immobilized at Fluorine-Doped Tin Oxide-TiO_2 Surfaces. *J. Phys. Chem. C* **2010**, *114*, 11822−11828.
(79) Wang, Q.; Zakeeruddin, S. M.; Nazeeruddin, M. K.; Humphry-Baker, R.; Grätzel, M. Molecular Wiring of Nanocrystals: NCS-Enhanced Cross-Surface Charge Transfer in Self-Assembled Ru-Complex Monolayer on Mesoscopic Oxide Films. *J. Am. Chem. Soc.* **2006**, *128*, 4446−4452.
(80) Ardo, S.; Meyer, G. J. Direct Observation of Photodriven Intermolecular Hole Transfer across TiO_2 Nanocrystallites: Lateral Self-Exchange Reactions and Catalyst Oxidation. *J. Am. Chem. Soc.* **2010**, *132*, 9283−9285.
(81) Patrick, C. E.; Giustino, F. O 1s Core-Level Shifts at the Anatase TiO_2(101)/N3 Photovoltaic Interface: Signature of H-Bonded Supramolecular Assembly. *Phys. Rev. B* **2011**, *84*, 085330.
(82) Johansson, E. M. J.; Hedlund, M.; Siegbahn, H.; Rensmo, H. Electronic and Molecular Surface Structure of Ru(tcterpy)$(NCS)_3$ and Ru(dcbpy)$_2(NCS)_2$ Adsorbed from Solution onto Nanostructured TiO_2: A Photoelectron Spectroscopy Study. *J. Phys. Chem. B* **2005**, *109*, 22256−22263.
(83) Laskova, B.; Zukalova, M.; Kavan, L.; Chou, A.; Liska, P.; Wei, Z.; Bin, L.; Kubat, P.; Ghadiri, E.; Moser, J. E.; et al. Voltage Enhancement in Dye-Sensitized Solar Cell Using (001)-Oriented Anatase TiO_2 Nanosheets. *J. Solid. State. Electrochem.* **2012**, *16*, 2993−3001.
(84) O'Regan, B.; Xiaoe, L.; Ghaddar, T. Dye Adsorption, Desorption, and Distribution in Mesoporous TiO_2 Films, and Its Effects on Recombination Losses in Dye Sensitized Solar Cells. *Energy Environ. Sci.* **2012**, *5*, 7203−7215.
(85) Tatay, S.; Haque, S. A.; O'Regan, B.; Durrant, J. R.; Verhees, W. J. H.; Kroon, J. M.; Vidal-Ferran, A.; Gavina, P.; Palomares, E. Kinetic Competition in Liquid Electrolyte and Solid-State Cyanine Dye Sensitized Solar Cells. *J. Mater. Chem.* **2007**, *17*, 3037−3044.
(86) Ehret, A.; Stuhl, L.; Spitler, M. T. Spectral Sensitization of TiO_2 Nanocrystalline Electrodes with Aggregated Cyanine Dyes. *J. Phys. Chem. B* **2001**, *105*, 9960−9965.
(87) Wang, Z.-S.; Cui, Y.; Dan-oh, Y.; Kasada, C.; Shinpo, A.; Hara, K. Thiophene-Functionalized Coumarin Dye for Efficient Dye-Sensitized Solar Cells: Electron Lifetime Improved by Coadsorption of Deoxycholic Acid. *J. Phys. Chem. C* **2007**, *111*, 7224−7230.
(88) Kawasaki, M.; Aoyama, S. High Efficiency Photocurrent Generation by Two-Dimensional Mixed J-Aggregates of Cyanine Dyes. *Chem. Commun.* **2004**, 988−989.
(89) Khazraji, A. C.; Hotchandani, S.; Das, S.; Kamat, P. V. Controlling Dye (Merocyanine-540) Aggregation on Nanostructured TiO_2 Films. An Organized Assembly Approach for Enhancing the Efficiency of Photosensitization. *J. Phys. Chem. B* **1999**, *103*, 4693−4700.
(90) Sayama, K.; Tsukagoshi, S.; Hara, K.; Ohga, Y.; Shinpou, A.; Abe, Y.; Suga, S.; Arakawa, H. Photoelectrochemical Properties of J Aggregates of Benzothiazole Merocyanine Dyes on a Nanostructured TiO_2 Film. *J. Phys. Chem. B* **2002**, *106*, 1363−1371.
(91) Wang, Q.; Campbell, W. M.; Bonfantani, E. E.; Jolley, K. W.; Officer, D. L.; Walsh, P. J.; Gordon, K. C.; Humphry-Baker, R.; Nazeeruddin, M. K.; Grätzel, M. Efficient Light Harvesting by Using Green Zn-Porphyrin-Sensitized Nanocrystalline TiO_2 Films. *J. Phys Chem. B* **2005**, *109*, 15397−15409.
(92) Lee, C.-W.; Lu, H.-P.; Lan, C.-M.; Huang, Y.-L.; Liang, Y.-R.; Yen, W.-N.; Liu, Y.-C.; Lin, Y.-S.; Diau, E. W.-G.; Yeh, C.-Y. Novel

Zinc Porphyrin Sensitizers for Dye-Sensitized Solar Cells: Synthesis and Spectral, Electrochemical, and Photovoltaic Properties. *Chem.—Eur. J.* **2009**, *15*, 1403−1412.
(93) Wang, P.; Zakeeruddin, S. M.; Comte, P.; Charvet, R.; Humphry-Baker, R.; Grätzel, M. Enhance the Performance of Dye-Sensitized Solar Cells by Co-grafting Amphiphilic Sensitizer and Hexadecylmalonic Acid on TiO_2 Nanocrystals. *J. Phys. Chem. B* **2003**, *107*, 14336−14341.
(94) Wang, M.; Li, X.; Lin, H.; Pechy, P.; Zakeeruddin, S. M.; Grätzel, M. Passivation of Nanocrystalline TiO_2 Junctions by Surface Adsorbed Phosphinate Amphiphiles Enhances the Photovoltaic Performance of Dye Sensitized Solar Cells. *Dalton Trans.* **2009**, *45*, 10015−10020.
(95) Kay, A.; Gratzel, M. ArtificialPhotosynthesis. 1. Photo-sensitizationof TiO_2 Solar Cells with Chlorophyll Derivatives and Related Natural Porphyrins. *J. Phys. Chem.* **1993**, *97*, 6272−6277.
(96) Horiuchi, T.; Miura, H.; Uchida, S. Highly-Efficient Metal-Free Organic Dyes for Dye-Sensitized Solar Cells. *Chem. Commun.* **2003**, 3036−3037.
(97) Hara, K.; Dan-oh, Y.; Kasada, C.; Ohga, Y.; Shinpo, A.; Suga, S.; Sayama, K.; Arakawa, H. Effect of Additives on the Photovoltaic Performance of Coumarin-Dye-Sensitized Nanocrystalline TiO_2 Solar Cells. *Langmuir* **2004**, *20*, 4205−4210.
(98) Yum, J.-H.; Jang, S.-r.; Humphry-Baker, R.; Grätzel, M.; Cid, J.-J.; Torres, T.; Nazeeruddin, M. K. Effect of Coadsorbent on the Photovoltaic Performance of Zinc Pthalocyanine-Sensitized Solar Cells. *Langmuir* **2008**, *24*, 5636−5640.
(99) Yum, J.-H.; Hardin, B. E.; Hoke, E. T.; Baranoff, E.; Zakeeruddin, S. M.; Nazeeruddin, M. K.; Torres, T.; McGehee, M. D.; Grätzel, M. Incorporating Multiple Energy Relay Dyes in Liquid Dye-Sensitized Solar Cells. *Chem. Phys. Chem.* **2011**, *12*, 657−661.
(100) Hardin, B. E.; Sellinger, A.; Moehl, T.; Humphry-Baker, R.; Moser, J.-E.; Wang, P.; Zakeeruddin, S. M.; Grätzel, M.; McGehee, M. D. Energy and Hole Transfer between Dyes Attached to Titania in Cosensitized Dye-Sensitized Solar Cells. *J. Am. Chem. Soc.* **2011**, *133*, 10662−10667.
(101) Jeong, N. C.; Son, H.-J.; Prasittichai, C.; Lee, C. Y.; Jensen, R. A.; Farha, O. K.; Hupp, J. T. Effective Panchromatic Sensitization of Electrochemical Solar Cells: Strategy and Organizational Rules for Spatial Separation of Complementary Light Harvesters on High-Area Photoelectrodes. *J. Am. Chem. Soc.* **2012**, *134*, 19820−19827.
(102) Etgar, L.; Park, J.; Barolo, C.; Lesnyak, V.; Panda, S. K.; Quagliotto, P.; Hickey, S. G.; Nazeeruddin, M. K.; Eychmüller, A.; Viscardi, G.; et al. Enhancing the Efficiency of a Dye Sensitized Solar Cell Due to the Energy Transfer Between CdSe Quantum Dots and a Designed Squaraine Dye. *RSC Adv.* **2012**, *2*, 2748−2752.
(103) Hoke, E. T.; Hardin, B. E.; McGehee, M. D. Modeling the Efficiency of Förster Resonant Energy Transfer from Energy Relay Dyes in Dye-Sensitized Solar Cells. *Opt. Express* **2010**, *18*, 3893−3904.
(104) Föster, T. 10th Spiers Memorial Lecture. Transfer Mechanisms of Electronic Excitation. *Discuss. Faraday Soc.* **1959**, *27*, 7−17.
(105) Pastore, M.; De Angelis, F. First-Principles Computational Modeling of Fluorescence Resonance Energy Transfer in Co-Sensitized Dye Solar Cells. *J. Phys. Chem. Lett.* **2012**, *3*, 2146−2153.
(106) De Angelis, F.; Fantacci, S.; Sgamellotti, A. An Integrated Computational Tool for the Study of the Optical Properties of Nanoscale Devices: Application to Solar Cells and Molecular Wires. *Theor. Chem. Acc.* **2007**, *117*, 1093−1104.
(107) Lee, D. H.; Lee, M. J.; Song, H. M.; Song, B. J.; Seo, K. D.; Pastore, M.; Anselmi, C.; Fantacci, S.; De Angelis, F.; Nazeeruddin, M. K.; et al. Organic Dyes Incorporating Low-Band-Gap Chromophores based on π-Extended Benzothiadiazole for Dye-Sensitized Solar Cells. *Dyes Pigm.* **2011**, *91*, 192−198.
(108) Kristyán, S.; Pulay, P. Can (Semi)Local Density Functional Theory Account for the London Dispersion Forces? *Che. Phys. Lett.* **1994**, *229*, 175−180.
(109) Tkatchenko, A.; Romaner, L.; Hofmann, O. T.; Zojer, E.; Ambrosch-Draxl, C.; Scheffler, M. Van der Waals Interactions Between Organic Adsorbates and at Organic/Inorganic Interfaces. *MRS Bull.* **2010**, *35*, 435−442.
(110) Johnson, E. R.; Mackie, I. D.; DiLabio, G. A. Dispersion Interactions in Density-Functional Theory. *J. Phys. Org. Chem.* **2009**, *22*, 1127−1135.
(111) Johnson, E. R. J.; Wolkow, R. A.; DiLabio, G. A. Application of 25 Density Functionals to Dispersion-Bound Homomolecular Dimers. *Chem. Phys. Lett.* **2004**, *394*, 334−338.
(112) Klimeš, J.; Michaelides, A. Perspective: Advances and Challenges in Treating van der Waals Dispersion Forces in Density Functional Theory. *J. Chem. Phys.* **2012**, *137*, 120901.
(113) Zhao, Y.; Truhlar, D. G. Benchmark Databases for Nonbonded Interactions and Their Use To Test Density Functional Theory. *J. Chem. Theor. Comput.* **2005**, *1*, 415−432.
(114) Zhao, Y.; Schultz, N. E.; Truhlar, D. G. Design of Density Functionals by Combining the Method of Constraint Satisfaction with Parametrization for Thermochemistry, Thermochemical Kinetics, and Noncovalent Interactions. *J. Chem. Theor. Comput.* **2006**, *2*, 364−382.
(115) Zhao, Y.; Truhlar, D. G. The M06 Suite of Density Functionals for Main Group Thermochemistry, Thermochemical Kinetics, Noncovalent Interactions, Excited States, and Transition Elements: Two New Functionals and Systematic Testing of Four M06-Class Functionals and 12 Other Functionals. *Theor. Chem. Acc.* **2008**, *120*, 215−241.
(116) Wu, Q.; Yang, W. Empirical Correction to Density Functional Theory for van der Waals Interactions. *J. Chem. Phys.* **2002**, *116*, 515.
(117) Grimme, S. Accurate Description of van der Waals Complexes by Density Functional Theory Including Empirical Corrections. *J. Comput. Chem.* **2004**, *25*, 1463−1473.
(118) Elstner, M.; Hobza, P.; Frauenheim, T.; Suhai, S.; Kaxiras, E. Hydrogen Bonding and Stacking Interactions of Nucleic Acid Base Pairs: A Density-Functional-Theory Based Treatment. *J . Chem. Phys.* **2001**, *114*, 5149.
(119) Zimmerli, U.; Parrinello, M.; Koumoutsakos, P. Dispersion Corrections to Density Functionals for Water Aromatic Interactions. *J. Chem. Phys.* **2004**, *120*, 2693.
(120) Grimme, S.; Antony, J.; Ehrlich, S.; Krieg, H. A Consistent and Accurate Ab Initio Parametrization of Density Functional Dispersion Correction (DFT-D) for the 94 Elements H−Pu. *J. Chem. Phys.* **2010**, *132*, 154104.
(121) Grimme, S. Semiempirical GGA-Type Density Functional Constructed With a Long-Range Dispersion Correction. *J. Comput. Chem.* **2006**, *27*, 1787−1799.
(122) Chai, J.-D.; Head-Gordon, M. Long-Range Corrected Hybrid Density Functionals with Damped Atom−Atom Dispersion Corrections. *Phys . Chem. Chem. Phys.* **2008**, *10*, 6615−6620.
(123) Grimme, S.; Ehrlich, S.; Goerigk, L. Effect of the Damping Function in Dispersion Corrected Density Functional Theory. *J. Comput. Chem.* **2011**, *32*, 1456−1465.
(124) Nara, M.; Torii, H.; Tasumi, M. Correlation between the Vibrational Frequencies of the Carboxylate Group and the Types of Its Coordination to a Metal Ion: An Ab Initio Molecular Orbital Study. *J. Phys. Chem.* **1996**, *100*, 19812−19817.
(125) Deacon, G. B.; Phillips, R. J. Relationships Between the Carbon−Oxygen Stretching Frequencies of Carboxylato Complexes and the Type of Carboxylate Coordination. *Coord. Chem. Rev.* **1980**, *33*, 227−250.
(126) Fantacci, S.; De Angelis, F. A Computational Approach to the Electronic and Optical Properties of Ru(II) and Ir(III) Polypyridyl Complexes: Applications to DSC, OLED and NLO. *Coord. Chem. Rev.* **2011**, *255*, 2704−2726.
(127) Martsinovich, N.; Troisi, A. Theoretical Studies of Dye-Sensitised Solar Cells: From Electronic Structure to Elementary Processes. *Energy Environ. Sci.* **2011**, *4*, 4473−4495.
(128) Shklover, V.; Ovchinnikov, Y. E.; Braginsky, L. S.; Zakeeruddin, S. M.; Grätzel, M. Structure of Organic/Inorganic Interface in Assembled Materials Comprising Molecular Components. Crystal Structure of the Sensitizer Bis[(4,4′-carboxy-2,2′-bipyridine)-(thiocyanato)]ruthenium(II). *Chem. Mater.* **1998**, *10*, 2533−2541.

(129) De Angelis, F.; Fantacci, S.; Selloni, A.; Nazeeruddin, M. K.; Grätzel, M. Time-Dependent Density Functional Theory Investigations on the Excited States of Ru(II)-Dye-Sensitized TiO_2 Nanoparticles: The Role of Sensitizer Protonation. *J. Am. Chem. Soc.* **2007**, *129*, 14156−14157.
(130) De Angelis, F.; Fantacci, S.; Selloni, A.; Grätzel, M.; Nazeeruddin, M. K. Influence of the Sensitizer Adsorption Mode on the Open-Circuit Potential of Dye-Sensitized Solar Cells. *Nano Lett.* **2007**, *7*, 3189−3195.
(131) Srinivas, K.; Yesudas, K.; Bhanuprakash, K.; Rao, V. J.; Giribabu, L. A Combined Experimental and Computational Investigation of Anthracene Based Sensitizers for DSSC: Comparison of Cyanoacrylic and Malonic Acid Electron Withdrawing Groups Binding onto the TiO_2 Anatase (101) Surface. *J. Phys. Chem. C* **2009**, *113*, 20117−20126.
(132) Schiffmann, F.; VandeVondele, J.; Hutter, J. r.; Wirz, R.; Urakawa, A.; Baiker, A. Protonation-Dependent Binding of Ruthenium Bipyridyl Complexes to the Anatase(101) Surface. *J. Phys. Chem. C* **2010**, *114*, 8398−8404.
(133) Pérez León, C.; Kador, L.; Peng, B.; Thelakkat, M. Characterization of the Adsorption of Ru-bpy Dyes on Mesoporous TiO_2 Films with UV−Vis, Raman, and FTIR Spectroscopies. *J. Phys. Chem. B* **2006**, *110*, 8723−8730.
(134) Chen, P.; Yum, J. H.; Angelis, F. D.; Mosconi, E.; Fantacci, S.; Moon, S.-J.; Baker, R. H.; Ko, J.; Nazeeruddin, M. K.; Grätzel, M. High Open-Circuit Voltage Solid-State Dye-Sensitized Solar Cells with Organic Dye. *Nano Lett.* **2009**, *9*, 2487−2492.
(135) De Angelis, F.; Fantacci, S.; Selloni, A.; Nazeeruddin, M. K.; Grätzel, M. First-Principles Modeling of the Adsorption Geometry and Electronic Structure of Ru(II) Dyes on Extended TiO_2 Substrates for Dye-Sensitized Solar Cell Applications. *J. Phys. Chem. C* **2010**, *114*, 6054−6061.
(136) De Angelis, F.; Fantacci, S.; Mosconi, E.; Nazeeruddin, M. K.; Grätzel, M. Absorption Spectra and Excited State Energy Levels of the N719 Dye on TiO_2 in Dye-Sensitized Solar Cell Models. *J . Phys. Chem. C* **2011**, *115*, 8825−8831.
(137) Rocca, D.; Gebauer, R.; De Angelis, F.; Nazeeruddin, M. K.; Baroni, S. Time-Dependent Density Functional Theory Study of Squaraine Dye-Sensitized Solar Cells. *Chem. Phys. Lett.* **2009**, *475*, 49−53.
(138) Martsinovich, N.; Jones, D. R.; Troisi, A. Electronic Structure of TiO_2 Surfaces and Effect of Molecular Adsorbates Using Different DFT Implementations. *J. Phys. Chem. C* **2010**, *114*, 22659−22670.
(139) Martsinovich, N.; Troisi, A. High-Throughput Computational Screening of Chromophores for Dye-Sensitized Solar Cells. *J. Phys. Chem. C* **2011**, *115*, 11781−11792.
(140) De Angelis, F. Direct vs. Indirect Injection Mechanisms in Perylene Dye-Sensitized Solar Cells: A DFT/TDDFT Investigation. *Chem. Phys. Lett.* **2010**, *493*, 323−327.
(141) Persson, P.; Bergstrom, R.; Lunell, S. Quantum Chemical Study of Photoinjection Processes in Dye-Sensitized TiO_2 Nanoparticles. *J. Phys. Chem. B* **2000**, *104*, 10348−10351.
(142) Vittadini, A.; Selloni, A.; Rotzinger, F. P.; Grätzel, M. Formic Acid Adsorption on Dry and Hydrated TiO_2 Anatase (101) Surfaces by DFT Calculations. *J. Phys. Chem. B* **2000**, *104*, 1300−1306.
(143) Tian, H.; Yang, X.; Chen, R.; Zhang, R.; Hagfeldt, A.; Sun, L. Effect of Different Dye Baths and Dye-Structures on the Performance of Dye-Sensitized Solar Cells Based on Triphenylamine Dyes. *J. Phys. Chem. C* **2008**, *112*, 11023−11033.
(144) Pastore, M.; De Angelis, F. Computational Modeling of Stark Effects in Organic Dye-Sensitized TiO_2 Heterointerfaces. *J. Phys. Chem. Lett.* **2011**, *2*, 1261−1267.
(145) Nunzi, F.; De Angelis, F. DFT Investigations of Formic Acid Adsorption on Single-Wall TiO_2 Nanotubes: Effect of the Surface Curvature. *J. Phys. Chem. C* **2011**, *115*, 2179−2186.
(146) Labat, F.; Adamo, C. Bi-isonicotinic Acid on Anatase (101): Insights from Theory. *J. Phys. Chem. C* **2007**, *111*, 15034−15042.
(147) De Angelis, F.; Fantacci, S.; Selloni, A.; Nazeeruddin, M. K.; Grätzel, M. First-Principles Modeling of the Adsorption Geometry and Electronic Structure of Ru(II) Dyes on Extended TiO_2 Substrates for Dye-Sensitized Solar Cell Applications. *J. Phys. Chem. C* **2010**, *114*, 6054−6061.
(148) Sodeyama, K.; Sumita, M.; O'Rourke, C.; Terranova, U.; Islam, A.; Han, L.; Bowler, D. R.; Tateyama, Y. Protonated Carboxyl Anchor for Stable Adsorption of Ru N749 Dye (Black Dye) on a TiO_2 Anatase (101) Surface. *J. Phys Chem. Lett.* **2012**, *3*, 472−477.
(149) Mosconi, E.; Selloni, A.; De Angelis, F. Solvent Effects on the Adsorption Geometry and Electronic Structure of Dye-Sensitized TiO_2: A First-Principles Investigation. *J. Phys. Chem. C* **2012**, *116*, 5932−5940.
(150) Horiuchi, T.; Miura, H.; Sumioka, K.; Uchida, S. High Efficiency of Dye-Sensitized Solar Cells Based on Metal-Free Indoline Dyes. *J. Am. Chem. Soc.* **2004**, *126*, 12218−12219.
(151) Ardo, S.; Sun, Y.; Castellano, F. N.; Meyer, G. J. Excited-State Electron Transfer from Ruthenium-Polypyridyl Compounds to Anatase TiO_2 Nanocrystallites: Evidence for a Stark Effect. *J. Phys. Chem. B* **2010**, *114*, 14596−14604.
(152) Ardo, S.; Sun, Y.; Staniszewski, A.; Castellano, F. N.; Meyer, G. J. Stark Effects after Excited-State Interfacial Electron Transfer at Sensitized TiO_2 Nanocrystallites. *J. Am. Chem. Soc.* **2010**, *132*, 6696−6709.
(153) Cappel, U. B.; Feldt, S. M.; Schoneboom, J.; Hagfeldt, A.; Boschloo, G. The Influence of Local Electric Fields on Photoinduced Absorption in Dye-Sensitized Solar Cells. *J. Am. Chem. Soc.* **2010**, *132*, 9096−9101.
(154) Staniszewski, A.; Ardo, S.; Sun, Y.; Castellano, F. N.; Meyer, G. J. Slow Cation Transfer Follows Sensitizer Regeneration at Anatase TiO_2 Interfaces. *J. Am. Chem. Soc.* **2008**, *130*, 11586−11587.
(155) Snaith, H. J.; Karthikeyan, C. S.; Petrozza, A.; Teuscher, J.; Moser, J. E.; Nazeeruddin, M. K.; Thelakkat, M.; Grätzel, M. High Extinction Coefficient "Antenna" Dye in Solid-State Dye-Sensitized Solar Cells: A Photophysical and Electronic Study. *J. Phys. Chem. C* **2008**, *112*, 7562−7566.
(156) Cappel, U. B.; Gibson, E. A.; Hagfeldt, A.; Boschloo, G. Dye Regeneration by Spiro-MeOTAD in Solid State Dye-Sensitized Solar Cells Studied by Photoinduced Absorption Spectroscopy and Spectroelectrochemistry. *J. Phys. Chem. C* **2009**, *113*, 6275−6281.
(157) Anderson, A. Y.; Barnes, P. R. F.; Durrant, J. R.; O'Regan, B. Simultaneous Transient Absorption and Transient Electrical Measurements on Operating Dye-Sensitized Solar Cells: Elucidating the Intermediates in Iodide Oxidation. *J. Phys. Chem. C* **2010**, *114*, 1953−1958.
(158) Cappel, U. B.; Smeigh, A. L.; Plogmaker, S.; Johansson, E. M. J.; Rensmo, H.; Hammarström, L.; Hagfeldt, A.; Boschloo, G. Characterization of the Interface Properties and Processes in Solid State Dye-Sensitized Solar Cells Employing a Perylene Sensitizer. *J. Phys. Chem. C* **2011**, *115*, 4345−4358.
(159) Stark, J. Observation of the Separation of Spectral Lines by an Electric Field. *Nature* **1914**, *401*, 401.
(160) Boxer, S. G. Stark Realities. *J. Phys. Chem. B* **2009**, *113*, 2972−2983.
(161) Bublitz, G. U.; Boxer, S. G. Stark Spectroscopy: Applications in Chemistry, Biology, and Materials Science. *Annu. Rev. Phys. Chem.* **1997**, *48*, 213−242.
(162) O'Rourke, C.; Bowler, D. R. Adsorption of Thiophene-Conjugated Sensitizers on TiO_2 Anatase (101). *J. Phys Chem. C* **2010**, *114*, 20240−20248.
(163) Mor, G. K.; Basham, J.; Paulose, M.; Kim, S.; Varghese, O. K.; Vaish, A.; Yoriya, S.; Grimes, C. A. High-Efficiency Förster Resonance Energy Transfer in Solid-State Dye Sensitized Solar Cells. *Nano Lett.* **2010**, *10*, 2387−2394.
(164) Wang, Z.-S.; Cui, Y.; Dan-oh, Y.; Kasada, C.; Shinpo, A.; Hara, K. Thiophene-Functionalized Coumarin Dye for Efficient Dye-Sensitized Solar Cells: Electron Lifetime Improved by Coadsorption of Deoxycholic Acid. *J. Phys. Chem. C* **2011**, *111*, 7224−7230.